REPORT DOCUMENTATION PAGE

Form Approved OMB NO. 0704-0188

1. REPORT DATE (DD-MM-YYYY)	2. REPORT TYPE	3. DATES COVERED (From - To)
30-09-2009	Final Report	1-Jun-2004 - 31-Jul-2008

4. TITLE AND SUBTITLE
Diagnostics of Flow Separation on Rotor Blades: Final Report

5a. CONTRACT NUMBER
W911NF-04-1-0184

5b. GRANT NUMBER

5c. PROGRAM ELEMENT NUMBER
611102

6. AUTHORS
Narayanan M. Komerath, Vrishank Raghav, James DiOttavio

5d. PROJECT NUMBER

5e. TASK NUMBER

5f. WORK UNIT NUMBER

7. PERFORMING ORGANIZATION NAMES AND ADDRESSES
Georgia Tech Research Corporation
Office of Sponsored Programs
Georgia Tech Research Corporation
Atlanta, GA 30332 -0415

8. PERFORMING ORGANIZATION REPORT NUMBER

9. SPONSORING/MONITORING AGENCY NAME(S) AND ADDRESS(ES)
U.S. Army Research Office
P.O. Box 12211
Research Triangle Park, NC 27709-2211

10. SPONSOR/MONITOR'S ACRONYM(S)
ARO

11. SPONSOR/MONITOR'S REPORT NUMBER(S)
46454-EG.3

12. DISTRIBUTION AVAILIBILITY STATEMENT
Approved for public release; distribution unlimited

13. SUPPLEMENTARY NOTES
The views, opinions and/or findings contained in this report are those of the author(s) and should not contrued as an official Department of the Army position, policy or decision, unless so designated by other documentation.

14. ABSTRACT
In a 4-year project, the radial flow phenomena in the stalled region of rotor blades typical of retreating-blade stall were investigated. First a partial inflow obstructor was devised in order to create transient flow separation on a rotor blade in a hover facility. Next, a 2-bladed teetering rotor rig was designed, built and operated at high advance ratios appropriate for dynamic stall, in the John Harper Low Speed Wind Tunnel at Georgia Tech. The nature of the flow induced near the surface by radial stresses in the stalled flowfield, was examined using Particle Image

15. SUBJECT TERMS
Radial flow, centrifugal effects, dynamic stall, rotor blade, Particle Image Velocimetry, Pressure Sensitive Paint, High Advance Ratio Facility

16. SECURITY CLASSIFICATION OF:			17. LIMITATION OF ABSTRACT	15. NUMBER OF PAGES	19a. NAME OF RESPONSIBLE PERSON
a. REPORT	b. ABSTRACT	c. THIS PAGE			Narayanan Komerath
U	U	U	SAR		19b. TELEPHONE NUMBER 404-894-3017

MAIN RESULTS

TABLE OF CONTENTS

1. OBJECTIVES

This project was a 1-year extension to a 3-year project on the three-dimensional flowfield on a rotor blade in dynamic stall. The 1-year extension allowed us to pursue unexpected results obtained with a new facility developed under the 3-year project. The long-term objectives of this research are:

1. Detailed mechanisms of retreating-blade stall on a helicopter rotor blade.
2. Free shear layer interactions related to the operation of leading-edge and trailing-edge devices on rotating blades.
3. Temporal evolution of flows and flow interactions relevant to active-control of separation and vortex interactions.

In the project reported here, the focus is on the first item; however, the basic knowledge and techniques developed here will be of benefit in addressing all of the others.

In the first phase over the past 3 years, we made substantial progress in developing facilities where hub-mounted diagnostics could be applied in future, and towards developing diagnostic instrumentation suited to that purpose. Having pushed that as far as present miniaturization of certain key components would allow, we focused on the fluid dynamics of the radial flow over rotor blades, behind the separation line in dynamic stall. This represents a largely unknown area in the research literature on dynamic stall related to helicopters (and to wind turbines).

2. SUMMARY OF PROGRESS TOWARDS LONG-TERM OBJECTIVES

1. Hub-mounted data acquisition

Two laptop computers small enough to be mounted on a 6” diameter rotor hub (Sony VAIO, micro laptop PC) were acquired. These could be operated on a rotating table at up to 200 rpm; however hard disc operation was intermittent because of acceleration-sensitive protection mechanisms. The entire data acquisition software could be placed on USB flash drives; however, system startup from these drives was not possible on the existing operating systems. The basic idea of operating with COTS hardware of this class was shown to be feasible. Communication with a device in the laboratory reference frame using wireless was also occurring, so that in principle, such a device could be commanded from a laboratory computer to start and stop data acquisition. Runs would have to be limited to the time available before the USB drives ran out of space, but with 2GB and 4GB drives, this is also not a major issue. With solid-state disks becoming available as main storage for micro-PCs over the past year, the operating system issue should disappear. Thus it should be possible in the near future to revisit this issue with computers that are not so acceleration-sensitive, and develop miniaturized blade-mounted diagnostic systems.

2. *Software-Based Counter Processor for Hub-Mounted Laser Velocimeter*

A counter-type processor of LV signals was successfully implemented in software and demonstrated using the micro-laptop PC to be used on the rotor hub. The counter was shown to work in the MegaHertz regime, needed for LV in the rotor application, using a signal generator. Tests with a rotating disc have also been commenced. Two difficulties with integrating this velocimeter with a rotating dynamic-stall experiment are:
a) the frequency shifter power supply and opto-electronics on this system are not robust enough to survive vibration, nor are they miniaturized.
b) the vibration level on our forward flight rotor setup during dynamic stall is not yet low enough to try this integration, even without the frequency shifting.

With recent developments, diode lasers have reached substantial power, and remain to be investigated for hub-mounted velocimetry systems. A 1watt miniature green diode laser has been acquired to enable exploration along these lines.

3. Pressure-Sensitive Paint Studies

The pressure-sensitive paint studies led to a peer-reviewed publication on high-response PSP. In the field of PSP, there are at least two frontiers: sensitivity and frequency response. The chemical requirements and surface preparation for each are quite different at present., and different paint formulations and surface textures are used. We pursued an opportunity for a breaktghrough in the frequency response arena: collaborating with Dr. Jim Gregory, then a PhD candidate in Prof, Sullivan's group at Purdue, to perform clean controlled experiments capturing the complex mode shape of a higher-order mode in an acoustic resonator. We have thus participated in pushing the frequency response frontier past 1600 Hz. The sensitivity frontier is still some distance away from reaching where we can use PSP in our present experiment, given the low rpm used.

4. Particle Image Velocimetry

Unlike laser Doppler velocimetry, where time-resolved velocity at a single point can be obtained in the blade-fixed reference frame, there is no advantage to using Particle Image Velocimetry (PIV) in the blade-fixed frame. The time between two successive velocity fields achievable with our systems is on the order of 30 milliseconds, at least one order of magnitude away from what can be achieved with LDV. So as the first stage of our long-term effort, we focused on using PIV. This was to look at the fluid mechanics of the radial flow over a rotor blade under transient stall conditions such as those encountered in dynamic stall. This followed the plan originally proposed.

As discussed below, this effort led to the discovery of some surprising features in the radial velocity field, whose further investigation is the subject of the present research. The progress towards the first objective, that of studying the radial flow in dynamic stall, is discussed in detail below.

3. ISSUES

The issues laid out in the original proposal are repeated here for the benefit of the reader who may not be familiar with the original proposal or the AIAA paper that resulted in 2006.

Full-Scale Dynamic Stall Problem

The high relative Mach numbers encountered on the advancing blade side (ABS) dictate the use of thin airfoils with small nose radius and a relatively flat upper surface to reduce shock drag and impulsive noise. As these blades pitch up on the RBS, the flow over the nosetip encounters large negative pressure coefficients (Cp of –5.4 shown at 0.5% chord (Ref.1), exacerbated by unsteady effects. Thus local Mach number reaches[9] as high as 1.3. Carr and colleagues (Ref.2) have shown effects of shocks in the development of dynamic stall.

Influence of spanwise flow on rotating blades

Bousman's data (Ref.3) show that moment stall begins at an early azimuth where the freestream has a substantial spanwise inboard-directed velocity component, whereas close to the surface, radial acceleration drives the boundary layer fluid outward along the span. This must generate a strong velocity gradient which changes rapidly as the spanwise component comes to zero at 270 degrees azimuth. Thus, the correct fluid dynamics problem to simulate in experiments to capture stall initiation/suppression appears to be one of three-dimensional separation over a yawed wing with high radial acceleration at the surface. High aspect ratio is a secondary consideration here.

Influence of radial acceleration

This has been debated in the literature some years back, but has generally not been given much attention due to the difficulty of conducting boundary layer measurements on rotating blades. Coton (Ref.4) cites the substantial differences in the inboard pressure distribution on rotating wind turbine blades compared to 2-D models, preceding dynamic stall. He also cites the delay in forward movement of the separation region (prior to lift-off of the dynamic lift vortex) due to spanwise flow. Corten (Ref. 5) has used a "stall flag" method to capture the occurrence of stall on full-scale wind turbine blades. His analysis shows that in the dynamic stall region, there is a substantial radial pressure gradient and accompanying radial flow. Corten also cites laser velocimeter results showing the formation of vorticity directed parallel to the rotor axis along the aft portions of the blade. Radial acceleration must have a strong influence on the lift and pitching moment evolution after stall occurs. Xu (Ref.6) shows that the influence of rotation (centrifugal effects in the boundary layer) on a wind turbine blade, when modeled using a full Navier-Stokes formulation, shows a substantial stall delay in the 3-D case compared to 2-D cases where there is no rotation effect.

Liou (Ref.7) compared laser velocimeter results for the same blade operated as a rotor in the 9' facility used in the first part of the present work, and as a fixed-wing with the appropriate inflow correction in the 7' x 9' low speed wind tunnel used for the forward flight experiments here. We found, in cross-flow measurements made at the blade trailing edge, a substantial radial flow induced in the separated zone, compared to the fixed-wing measurements. The flow over the same blade was measured, in a 9' rotor facility in "hover"

at pitch angles of 15 deg. and 30 deg. and then as a fixed-wing in the John Harper Wind tunnel. The angle of attack in the wind tunnel was set to correspond to the pitch angle, corrected for the averaged inflow from the rotor experiment. Thus the angles of attack in the wind tunnel were substantially lower. These studies illustrated some interesting features. At the trailing-edge cross-flow plane, the radial velocity was drastically different between the rotating and fixed tests. The effect of the radial flow in the boundary layer was clearly visible. Over the blade tip, the tip vortex was seen to form and burst, much like on a delta wing. The region of separated flow included a large “dead-air zone” where the flow moved essentially at the same mean velocity as the blade.

Influence of Pitch Rate

The influence of pitching can be broken up into that due to quasi-steady change in angle of attack, a vorticity convection effect, and the unsteady acceleration effect of the wall on the flow. The last of these is negligible at the low reduced-frequencies involved in the rotor cyclic pitch case. The “moving wall effect” is small in the rotorcraft case. In other words, an actual blade pitching rate is not essential to simulate the essential features of dynamic stall, if the effective angle of attack can be changed rapidly by other means.

To summarize the guidance from the above, we see that to study the issues discussed above, it is appropriate to use blades of low aspect ratio (because we are interested in the inboard flowfield, not so much the tip vortex). This allows us to obtain larger chord Reynolds number without going to high speed. There is no need to go to a Mach number high enough to simulate the compressible flowfield over the leading edge, because we are looking at the flow behind the stall line in the inboard region. The implication of not needing high pitch rate is that it becomes possible then to simulate transient stall conditions with a rotor in a much simpler hover facility, with no cyclic pitch. Transient stall is generated instead in that facility by obstructing the inflow over the region of interest. We do use cyclic pitch in the forward flight experiment.

4. **RESULTS FROM THE HOVER FACILITY EXPERIMENTS**

The following results are excerpted from AIAA Paper 2006-3377 (Ref. 8) presented in June 2006. The objective of this experiment was to study the flowfield behind the separation line on the inboard region of a rotating blade, and do so in a setup where hub-mounted instrumentation can be integrated into the system.

We used a single-bladed rotor in a hover facility, with the inflow obstructed over a sector to increase effective angle of attack suddenly. The rationale behind these experiments is that it is much simpler than conducting a wind tunnel forward flight rotor experiment, for flow diagnostics.

- Conditions of zero spanwise freestream flow can be studied, while maintaining the radial acceleration and high pitch angle features – a logical transition from non-rotating cases.
- Tangential and radial extents of the region of stall can be varied, without changing rpm.

The scope of the experiment was to verify that stall occurs in the obstructed region, and rotor remains unstalled over majority of the rotor disc outside the obstruction, and to explore the radial flow downstream of the separation line.

Facility Description

Parameters of the facility shown in Figures 1 and 2 are summarized in Table 1. The single-bladed rotor has a flap degree of freedom. The speed can be varied continuously from 0 to 1000 RPM. The constant chord, untwisted blade has a square, flat tip. The blade is statically balanced by a counterweight. The collective pitch can be manually adjusted, and the blade is free to flap within a small range of angles. A Hall Effect sensor sends a pulse to an external signal generator every time a tab on the rotor shaft passes, providing azimuth reference. A plate in the shape of a 60-degree sector is mounted upstream of the rotor disc as shown in Figure 1, in order to restrict the inflow velocity over that part of the disc.

The flow is seeded with atomized food-grade mineral oil used for laser velocimetry. The illumination source is a pair of pulsed Nd-YAG lasers, with coincident output beams, expanded into a laser sheet in the region of interest. A 10-bit Charged Couple Device (CCD) camera of 1360x1024 pixel resolution is used to obtain flow images pairs for Particle Image Velocimetry (PIV). Signal-to-noise ratio begins to degrade for particle displacements exceeding $1/4^{th}$ of the correlation window size. Measurements at 500 RPM were conducted with 50 microseconds pulse separation. Initial measurements were made in cross-sections at selected radial locations to capture the flow development over the airfoil section. To sense the radial velocity, the laser sheet was aligned with the radius, perpendicular to the rotor disc. The viewing region was a 13.76 cm (radial coordinate) x 11.23 cm (axial coordinate) rectangle. The CCD camera was located 38 cm from the axis of rotation, as shown in Figure 3.

Table 1: Inflow Obstruction Experiment Parameters

Blade radius = 0.61m
Blade chord = 0.13m
Aspect ratio = 4.8
Airfoil section: NACA 0012
Pitch link range: 0 to 18 deg.
Obstruction: >1.25R ; 60 deg. Sector blockage.
RPM range: 70 to 500.
Test Cell dimensions: 2.74x2.74x6.4 m.
Horizontal rotor shaft.
11.kw variable speed DC drive
Counterweight opposite rotor blade.

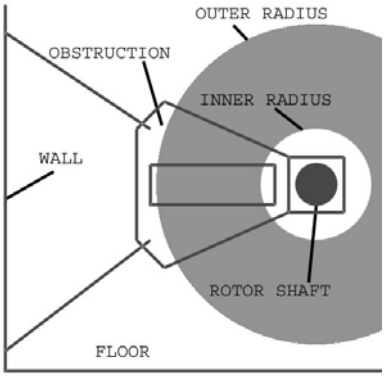

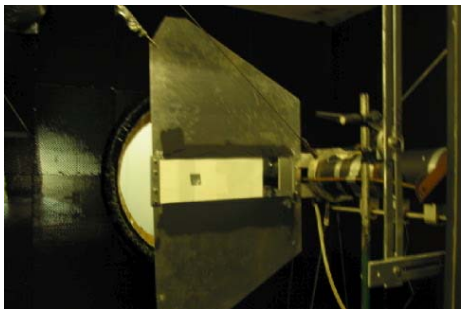

Figure 2: View from upstream

To sense the axial flow, the camera was positioned on the ceiling of the facility. For this experiment, 90 degrees azimuth corresponds to 19 mm from the leading edge of the blade. At 500 RPM, an azimuth increment of one degree would take 0.33 milliseconds at the blade tip. Steps of 1 degree were taken until 106 degrees azimuth, which is 25.4mm from the trailing edge. Radial velocity was captured at various locations along the spanwise viewing plane covering 137 mm of the blade about the 380 mm radial location as the center.

Results From the Obstructed Inflow Experiment

The blade operating conditions were set by reference to previous data (Ref. 7), and using Pulsed Laser Sheet Imaging (PLSI), at 15 deg. pitch, where the rotor is known to operate with attached flow, but very close to a stall condition at 500 rpm (30 m/s tip speed). With the obstruction installed, studies were conducted at 70 rpm. This was slow enough to capture successive video images, showing the same seeding during a single-event approach and passage of the blade through the seeding cloud, albeit at low Reynolds number. PLSI showed that the flow across the disc (axial velocity component), which should sharply accelerate as a lifting blade passes, was being stopped suddenly, indicating blade stall. The inflow during the rest of the rotor cycle was due to the lift generated when the blade was beyond the inflow-obstruction. This finding was quantified by PIV, with comparisons to the expected velocities from momentum inflow theory.

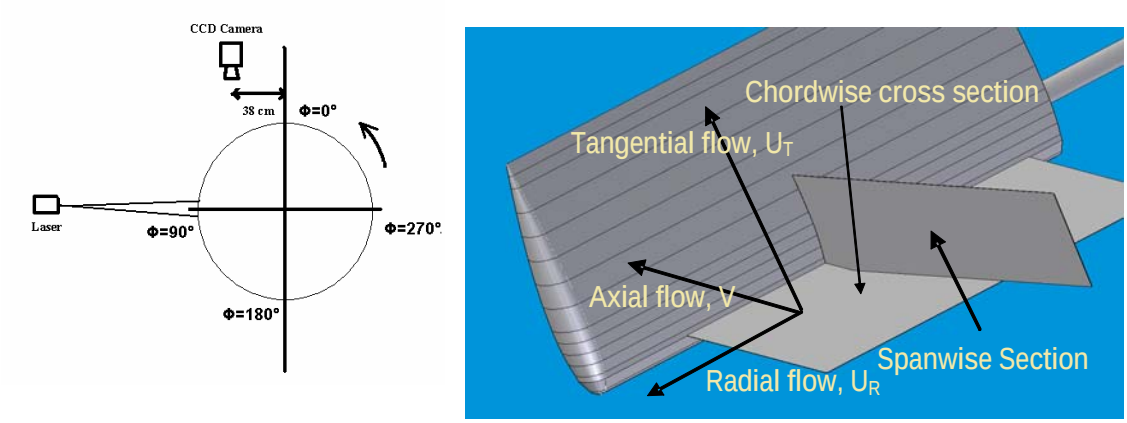

Camera orientation viewed from the suction side (up

Figure 3: Coordinate system and camera orientation

The surprising result was in the contours of axial and radial velocities in the stalled region, shown in Figure 4. Axial flow data showed that stall was indeed occurring. Further measurements suggest why strong radial outflow does not continue to develop along the blade as was expected from the sharp decrease in radial inflow at the edge of the recirculation region. Instantaneous velocity fields showed cells of spanwise recirculation separated by columnar flow structures, as schematically shown in Figure 4. It is important to distinguish the axial velocity directed away from the surface due to chordwise separation from axial flow due to the columnar flow structure and cells of spanwise separation. The extent of each flow structure is limited to only a couple of centimeters. The columnar flow is distinguished in contour plots of velocity by the presence of regions of opposite flow rotation on either side.

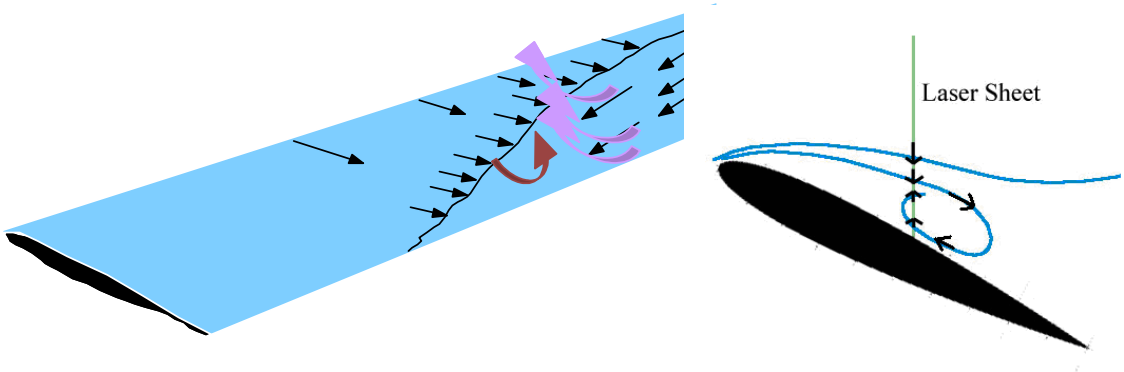

Figure 4: Schematic illustration of columnar structures in separated flow

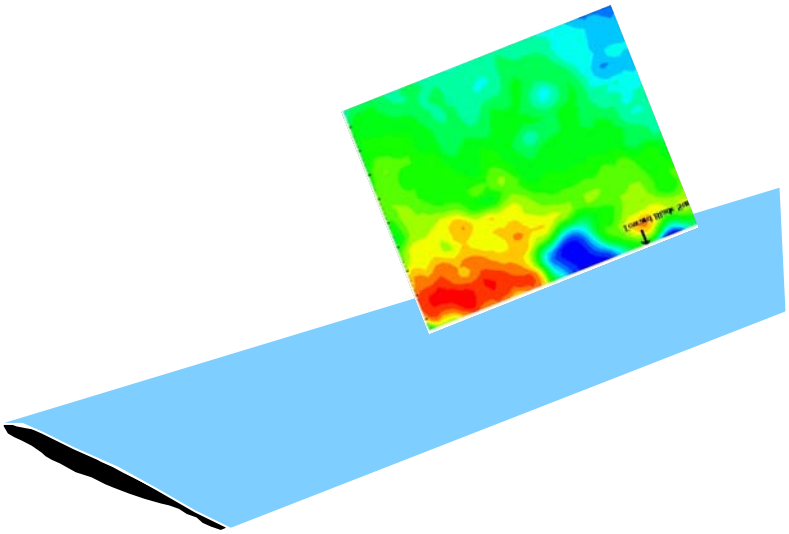

Figure 5: Contours of axial velocity showing that the radial velocity field is broken into discrete cells separated by regions of upward and downward axial flow.

Detailed velocity contour plots of the results are presented in AIAA Paper 2006-3377 (Ref.8). Figure 5 shows one instance, with contours of axial velocity. Red denotes a region where the flow is towards the blade surface, while blue denotes flow directed away from the surface. When several instances are viewed, basically the same behavior is observed in approximately the same locations; however, the phenomenon is not amenable to phase-locking with the rotor azimuth. Conclusions from the Inflow Obstructor experiment are summarized below.

1. A single-blade hover facility is used with an Inflow Obstructor plate to simulate the dynamic stall region downstream of the separation line.
2. PLIS and PIV confirm stall occurrence based on stoppage of the through-flow.
3. Downstream of the stall line, the radial velocity near the blade develops an outward direction. Stall cells along the radius exchange fluid away from the boundary layer.
4. The phase-locked radial velocity profile shows higher deceleration of radial out-flow from leading edge to chord-wise location where flow recirculation begins. This suggests that the inboard directed velocity of the upper surface flow dominates over the centrifugal effect, from the leading edge to separation point. Beyond separation, centrifugal flow dominates.
5. The cells of radial flow separation, comparable in scale to the blade chord, vary from cycle to cycle.

5. HIGH ADVANCE RATIO FACILITY

Figure 6: Dynamic Stall rig assembly in the test section of the John J. Harper wind tunnel.

ROTOR SPECIFICATIONS		
Blade Mass Total	1.752	**kg**
Blade Span	0.62	**m**
Blade Chord	0.178	**m**
Disc Radius	0.886	**m**
Solidity	0.0895	
Precone	1.6	**deg**
Max Collective	10	**deg**
Max Cyclic	6.5	**deg**
Max TPP Tilt	16	**deg**
Airfoil	NACA 0012	
Blade Aspect Ratio	3.49	
Motor HP	5	
Height	1.575	**m**

Table 2: Dynamic Stall Rotor Parameters

After reviewing options for designing a dynamic stall forward flight experiment rig, a teetering hub design was selected. This was to remove the need to "fly" the rotor to its operating condition, and instead be able to start the rotor and then the wind tunnel, and independently reach operating points. Fully articulated rotors would require "flying" from the control room to avoid disastrous conditions on the way to the operating point.

Since the setup is intended for aerodynamic/ flow diagnostic tests, blade elasticity is not an issue. We selected a 600 lb gross weight personal helicopter kit as the basis of the design. The main and tail rotor hubs and swashplates, as well as two NACA 0012 main rotor blades were acquired. The rotor blades are 6.55m in diameter, and operate at around 450 rpm. Thus the hub is built to take the centrifugal load under such conditions, and support over 2700N (600 lb) thrust in climb. One blade was cut to produce two model rotor blades, each 0.62m in span. Clearly the hub is safely designed for the present experiment operating range of 200 to 500 rpm. Pitch links were strengthened for the dynamic stall rig (Figure 6). Facility parameters are shown in Table 2.

6. RADIAL FLOW OVER THE BLADE IN FORWARD FLIGHT DYNAMIC STALL

The viewing plane used for flow visualization and PIV is shown schematically on a picture of the Retreating Blade Side (RBS) of the rotor in Figure 7. The camera is mounted upstream of, and below the 270 degrees azimuth. Operating conditions were selected by trial and error, varying collective and cyclic at selected advance ratio to verify the occurrence of dynamic stall. At 10 degrees collective and 5 degrees cyclic, flow visualization of the chordwise flowfield using mineral oil fog and a pulsed laser sheet verified stall over most of the blade at mid-radius. The images in Figure 7 suggest vortical structures in the stalled flow as the trailing edge of the blade passes the measurement plane.

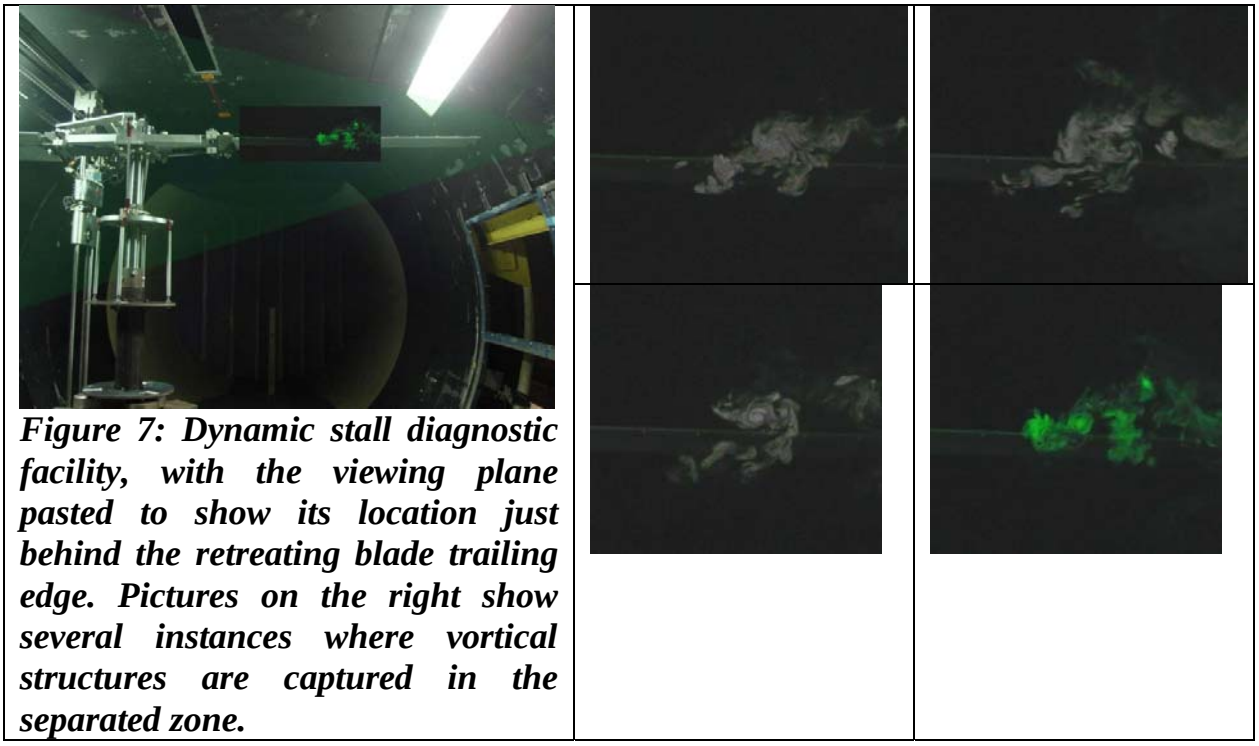

Figure 7: Dynamic stall diagnostic facility, with the viewing plane pasted to show its location just behind the retreating blade trailing edge. Pictures on the right show several instances where vortical structures are captured in the separated zone.

Figure 8 shows a sample velocity vector plot from instantaneous PIV data (100 microseconds between images), taken about 1 mm downstream of the trailing edge in the vertical/radial plane at 270 degrees rotor azimuth. There are clearly discrete zones of radial flow, though now there is no actual upflow in the trailing edge plane, unlike in the case with the inflow-obstructor experiment. Four oval-shaped regions are marked to indicate the discrete zones. Sampling of numerous such flowfield results showed that the number of discrete zones in the viewing plane was approximately 4 on average, i.e., the spacing between the structures was roughly constant. This spacing worked out to be roughly the same as the nominal height of the separated flow region at the trailing edge of the blade, suggesting discrete vortical structures occupying the stalled region. The average structure diameter is roughly 0.033m, while the height of the separated flow region is roughly 0.035-0.045m, calculated by assuming that separation occurs

roughly at the maximum thickness part of the blade at the given inclination angle. This lends credence to an approximate model of the dynamic stall flowfield as shown in Figure 9, where the separating shear layer rolls into discrete structures that grow with downstream distance.

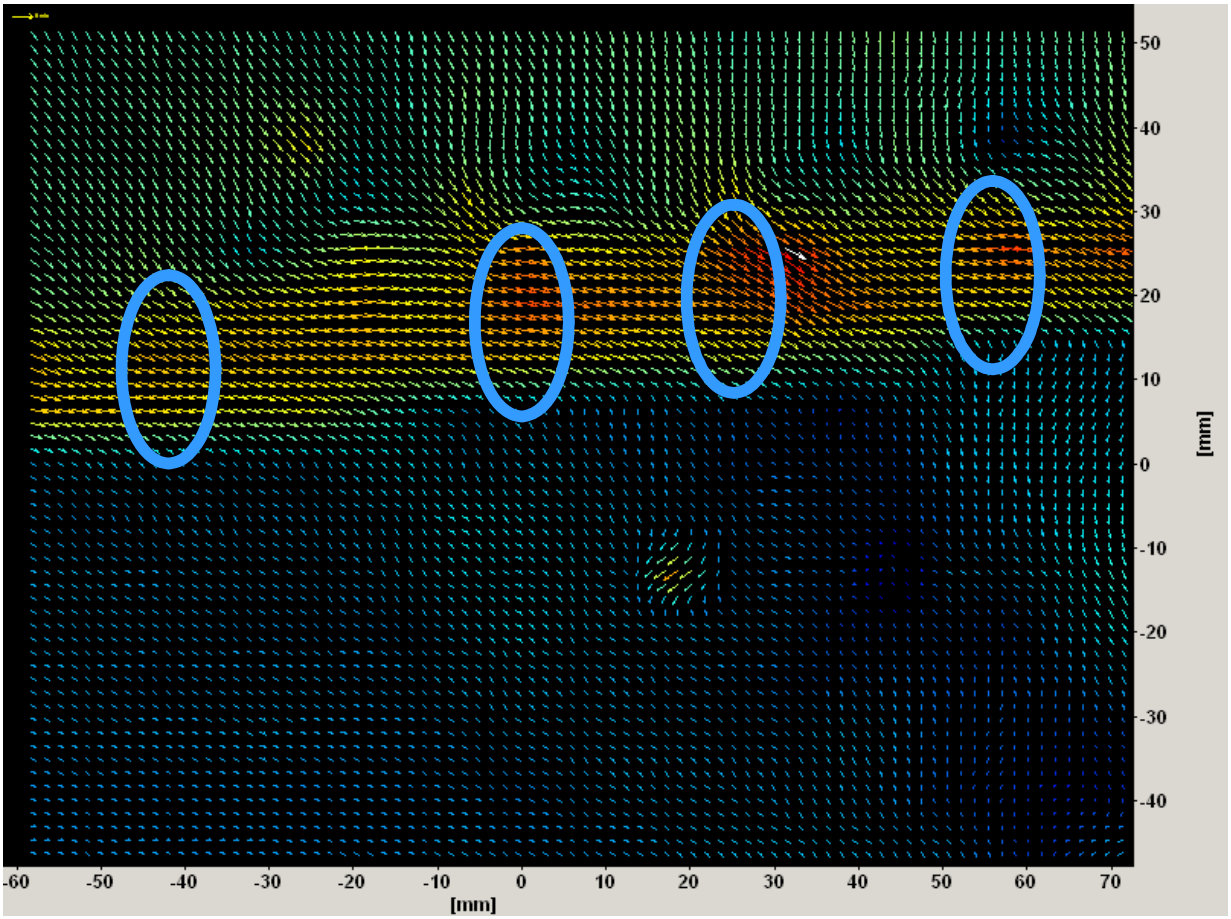

Figure 8: Velocity vectors in an axial-radial plane 1mm behind blade trailing edge at 270 deg. azimuth. 100 microseconds delay between PIV images. Red is highest magnitude. Blue ovals are drawn around discrete regions.

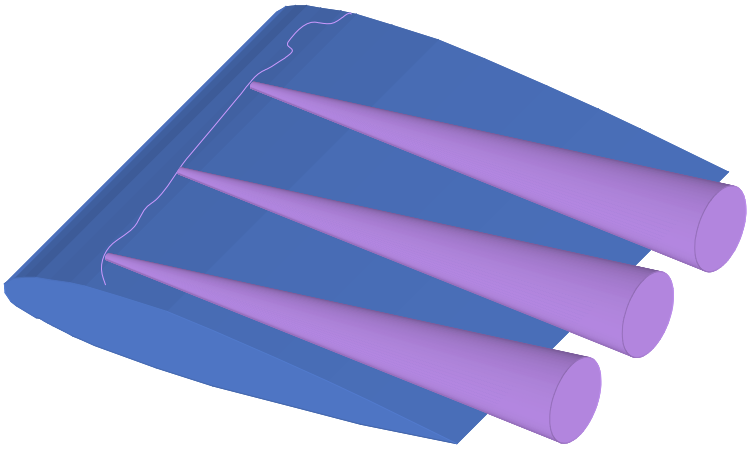

Figure 9: Schematic representation of discrete stall structures.

The PIV measurement window was moved in steps along the blade radius, and 100 image-pairs were captured at each position. The locations of these windows is shown in Fig. 10. The windows overlapped, as shown. To examine the radial velocity, three vertical lines were chosen in each window as shown. The radial velocity profile from individual (instantaneous, 100 microsecond) velocity fields, was extracted along each vertical line. Figure 11 shows a sample.

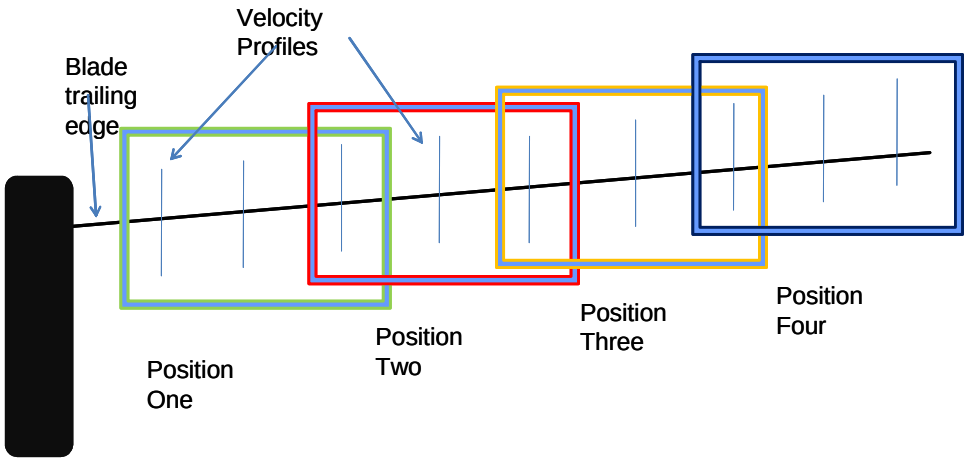

Figure 10: PIV windows along the blade trailing edge at 270 degrees azimuth.

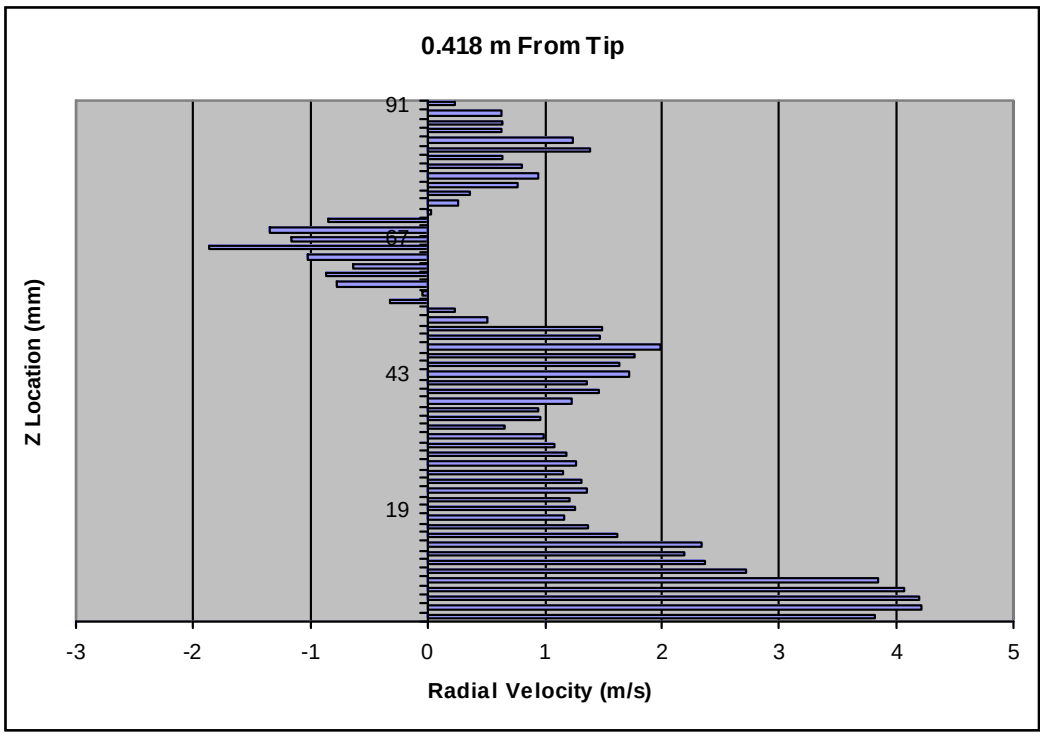

Figure 11: Profile of radial velocity at r/R=0.528, immediately behind the trailing edge at 270 deg. azimuth

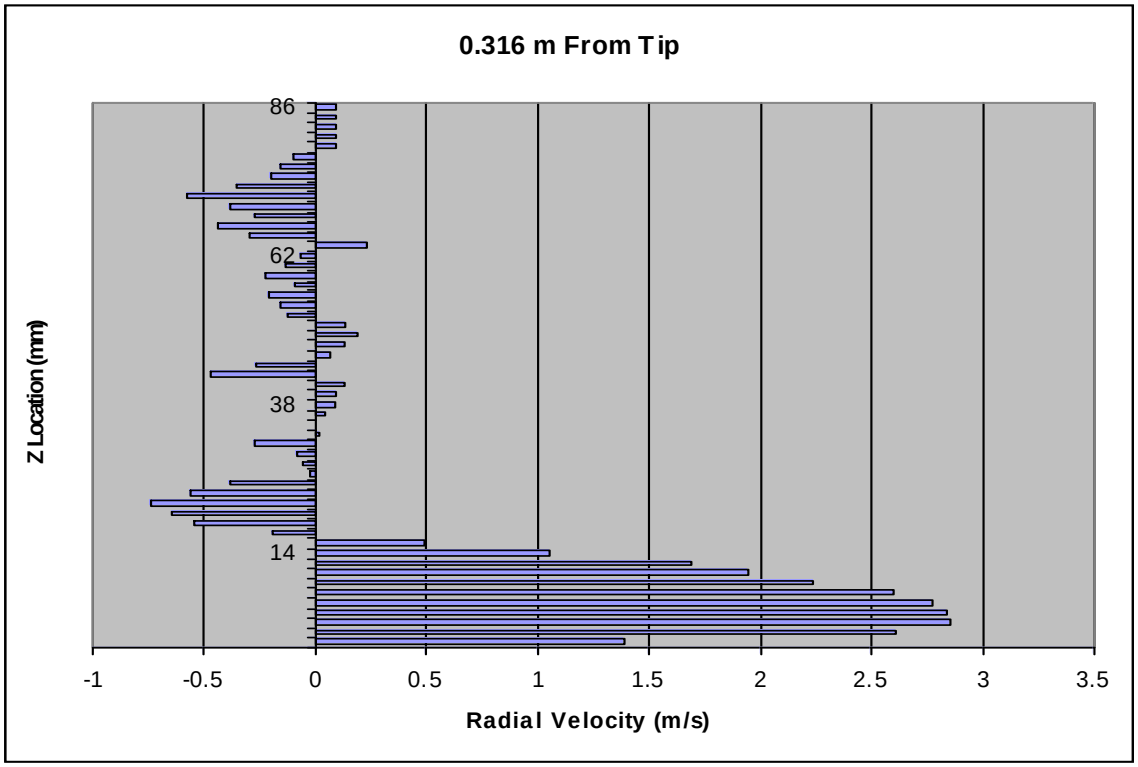

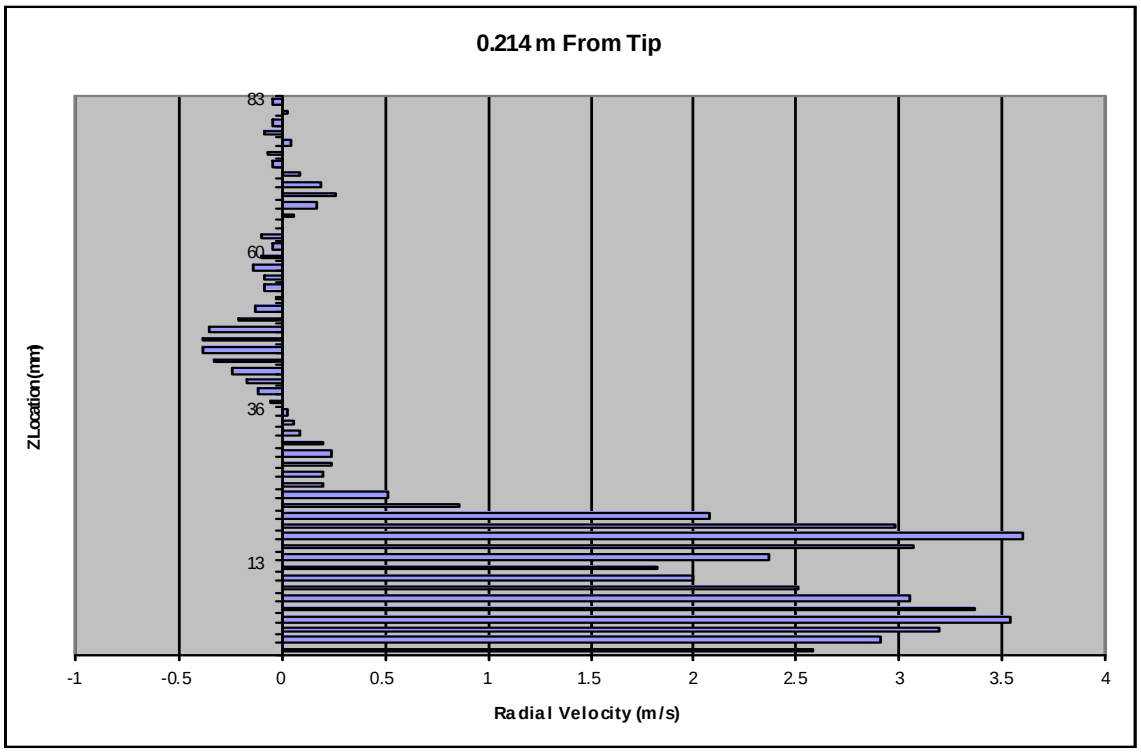

Figures 12(above) and 13 (below): Profiles of radial velocity at r/R=0.64 (Fig.12) and 0.758 (Fig.13), immediately behind the trailing edge at 270 deg. azimuth

Figure 11 shows the velocity profile at 0.418m from the tip, which corresponds to r/R= 0.528 for the rotor radius of 0.886m. The vertical axis is distance along the vertical (i.e., parallel to the rotor axis), and the range shown corresponds to $\Delta z/R$ of 0.102, or a $\Delta z/c$ = 0.51, for the blade chord of 0.178m. This is less than the height of the separated flow region, which is approximately 0.15 to 0.2R above the trailing edge. The bottom of the vertical axis is the blade trailing edge location. We see that the viscous boundary layer under the radial flow appears to have been partially captured. Above this thin region, the radial velocity profile reaches a peak, and then falls off. These features are qualitatively repeatable in all the images, however, the velocity field features above this region are not consistent from image to image. This is understandable for a separated flow region.

Figure 12 shows the profile at r/R = 0.643, and Figure 13 shows it at r/R = 0.758. The peak radial velocity is lower than that at the more inboard location. This is attributable to the formation of the stall cells that exchange the radial flowing fluid away from the blade surface, and to the fact that the tip region is not stalled. Thus the chordwise extent of stall may be expected to be smaller as one moves outboard (see Fig.4).

Similar trends persist out to r/R = 0.9, but at r/R=0.93, the tip vortex influence dominates. Figure 14 captures the tip vortex velocity field. At this condition, the tip vortex has a core diameter of approximately 0.16c, (or 1.33 times thickness), comparable to the expected 0.12c, if the core is the same size as the thickness of the airfoil. These are rough estimates. The center of the tip vortex is approximately at this location, as seen from Figure 15. However, the point is that the tip vortex is still fairly strong, indicating positive lift generation in the outboard region, whereas the inboard region is stalled. Again, substantial differences occur from one velocity field to another at the same blade azimuth (not shown here), above the radial flow region. This is to be expected, since it is a separated flowfield.

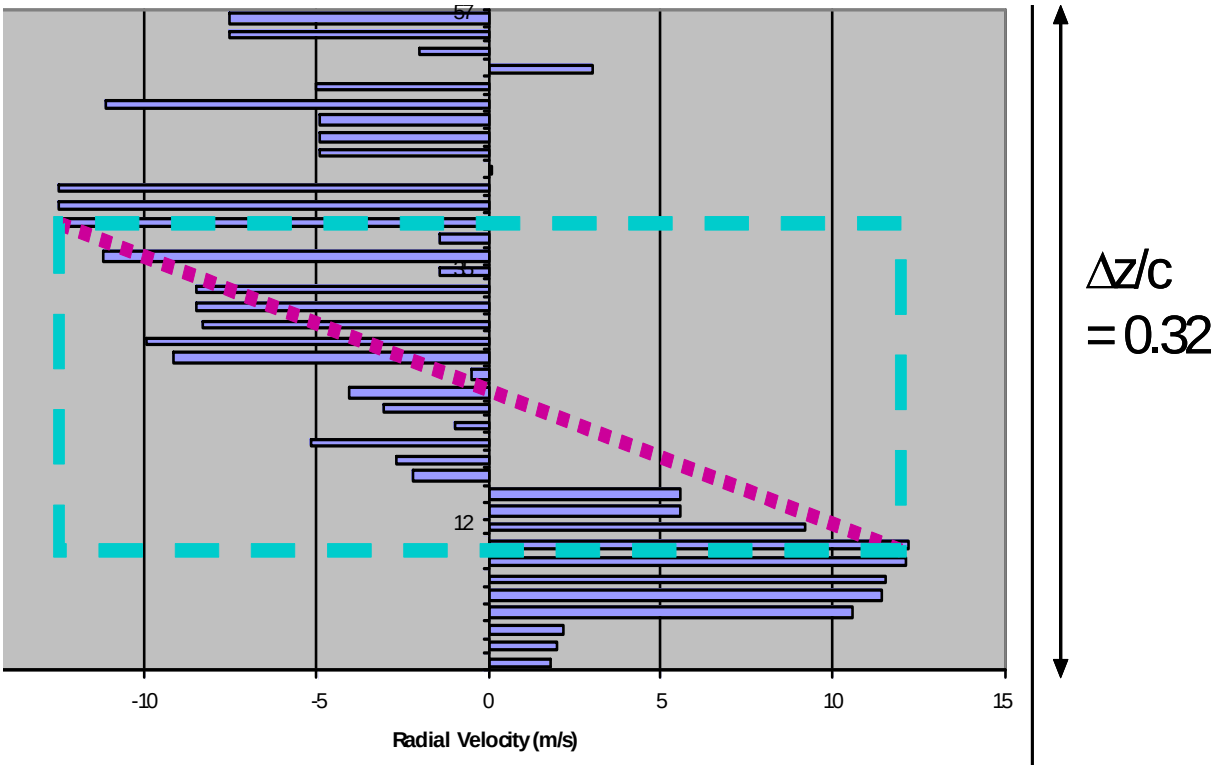

Figure 14: Radial velocity profile across the tip vortex

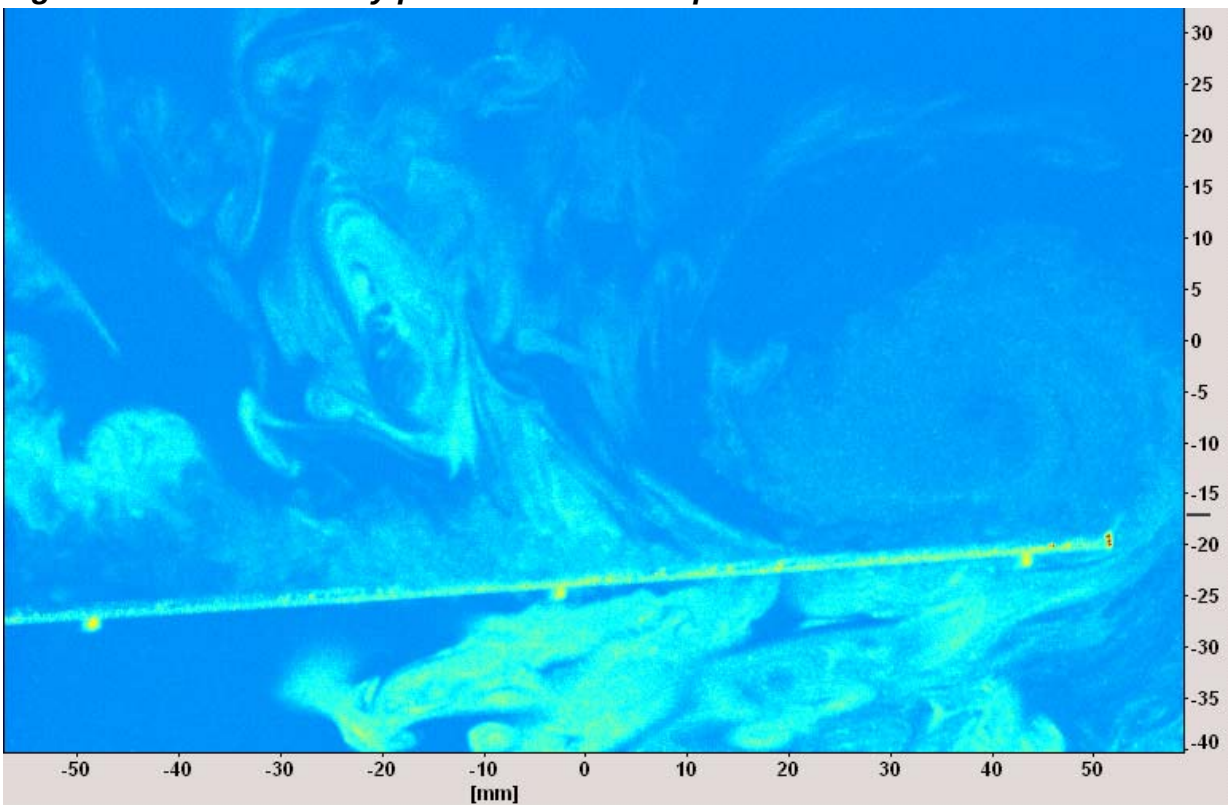

Figure 15: PLSI image showing tip vortex center at 11mm from the tip.

The above results raised interesting questions. A review of the literature on the nature of the separated flow over lifting surfaces, reveals very little on the dynamic stall flowfield, but does include some studies on stalled fixed-wings. The findings from these are briefly summarized below. Gregory et al (Ref.9) appear to be the first to have studied this flowfield, and detected three-dimensional flow patterns on airfoils. They based their observations on surface visualization, and were interested in the problem of obtaining two-dimensional characteristics in the presence of such three-dimensionality. Winkelmann and Barlow (Ref.10) extended these studies for a rectangular planform finite wing beyond stall, again focusing on the surface streaklines in oil flow visualization. Weihs and Katz (Ref. 11) reported cells in the post-stall flowfield over straight wings. Yon (Ref. 12) reported coherent structures in the wake of a stalled rectangular wing, and a NASA contractor report arising from Yon's PhD thesis, (Ref. 13), showed cells in the separated flow, and fluctuations attributed to these cells. The issue here was the separation of the flow over flaps, with a span/flap chord ratio of 2. There is no mention of spanwise flow here.

Boeren and Bragg (Ref. 14) did a systematic study of structures in the separated flow, and fluctuations due to these. They developed a classification based on whether the separation was a trailing-edge separation or a leading edge separation. They found low-frequency oscillations characteristic of leading edge separation, with a separation bubble growing aftward. In this case it was essentially 2 D separation. On the other hand, spanwise separation cells were seen to arise from trailing-edge separation, but this was mostly steady. Thus from the above, it appears that spanwise cells have been observed in the stalled flow over fixed wings, and even on nominally "2-D" airfoil test models. This raised two questions:

1. Is the radial flow on rotating blades an attenuating or driving influence on the formation of such discrete structures, and/or fluctuations?
2. How does this view of the radial flow affect separation and reattachment dynamics?

Result: Discrete Structures Come From the Radial Jet Layer
Jim DiOttavio (Ref. 15)answered the first question by analyzing the 100-odd image pairs in each PIV window shown in Figure 10. He sought the ensemble-averaged profile of radial velocity and the root mean square variation thereof, at 3 vertical lines in each window, and constructed radial variation results. The argument used for the initial hypothesis is as follows: If the radial flow is a stabilizing influence, then the rms fluctuation intensity in radial velocity should be higher in the region well above the wall, and low in the region where the strong radial flow exists. If the radial flow is a driver of instability, then high fluctuations should be seen in the regions of high radial velocity, nearer the wall. Figure 16 shows that at the most inboard position analyzed, the fluctuation level is small, and the fluctuation is least where the mean radial velocity profile is strongest. This suggests that the radial flow at its outset is highly stabilizing. However, the opposite result is seen in Figure 17 at an outboard location (still well inboard of the tip vortex influence). Now the RMS clearly peaks sharply where the mean radial velocity peaks. Data at other positions is somewhere in between these two results.

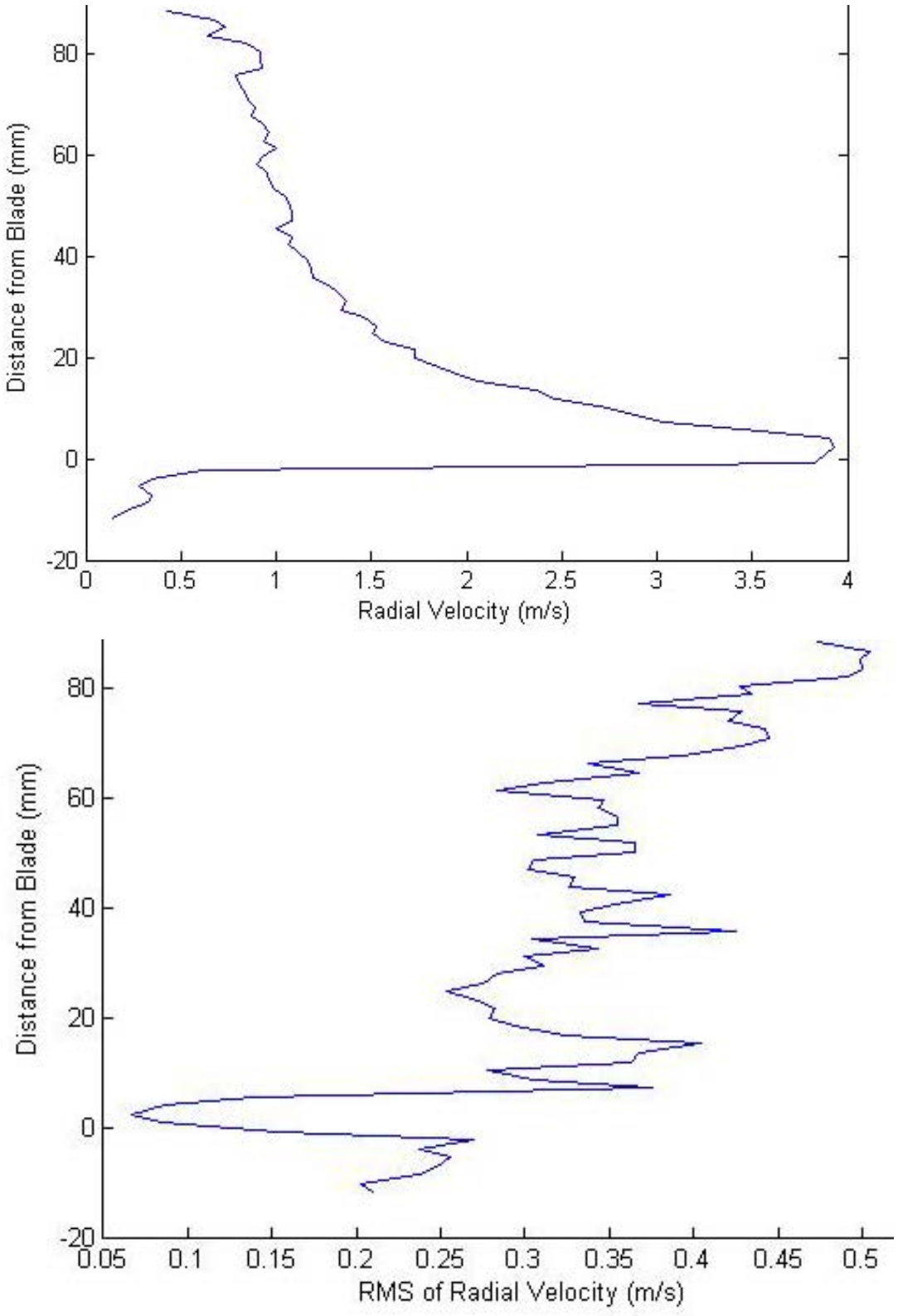

Figure 16: Profile of mean (above) and rms(below) radial velocity at r/R of 0.53

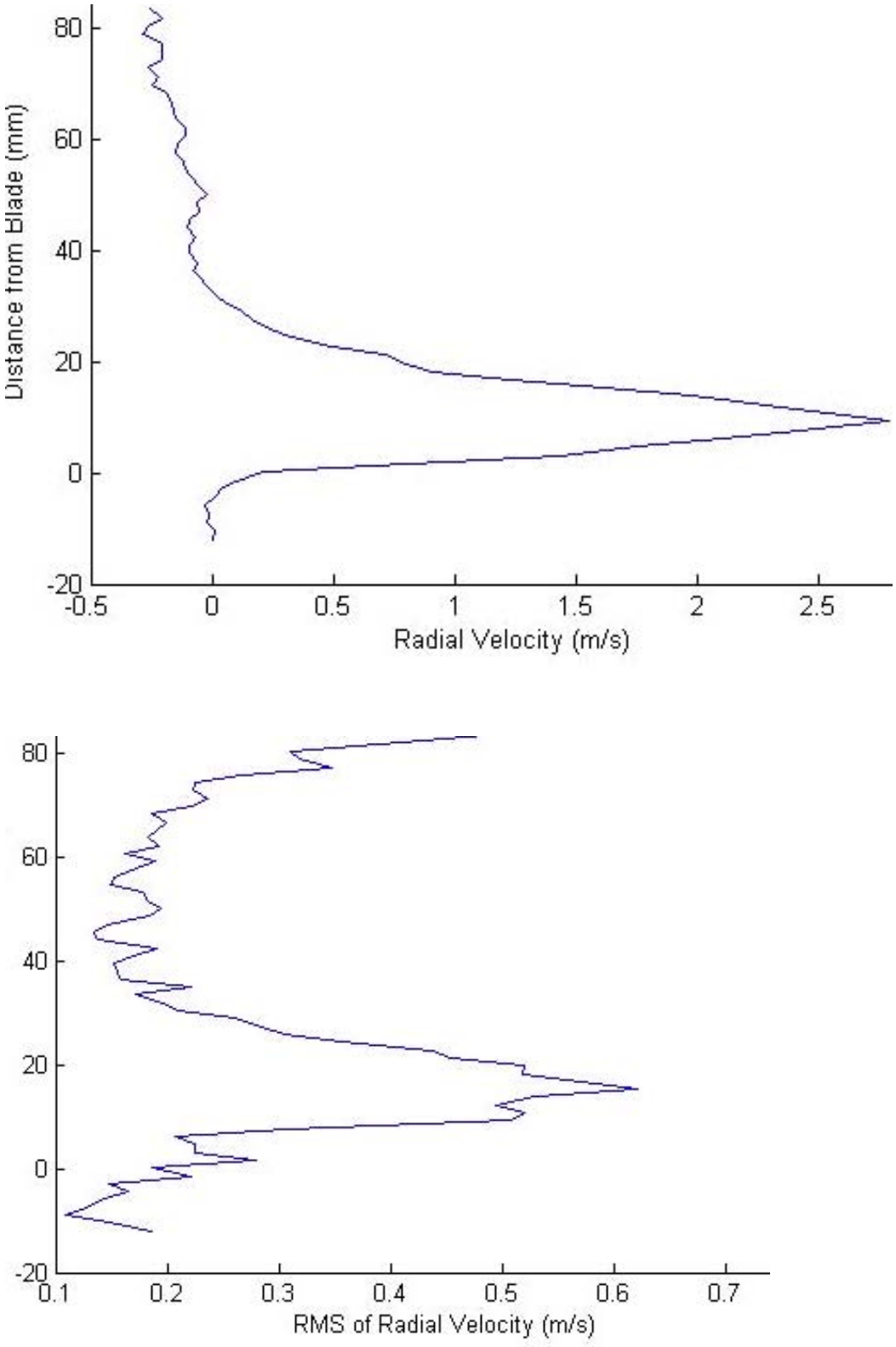

Figure 17: Mean and root-mean square radial velocity profiles at r/R=0.74, showing large rms coincident with the peak of mean radial velocity.

7. QUANTIFYING THE SIGNIFICANCE OF THE FINDINGS

The primary question that remained at the end of the 3-year initial project was regarding the significance of the findings to the computational prediction of loads during dynamic stall. To answer this, the results had to be carefully quantified. This was needed both to get quantitative measures of the vorticity in the structures relative to the relevant vorticity measures in the various sources of vorticity in the problem, and to be able to provide the data to computational researchers in order to make quantitative comparisons with computations done with various levels of modeling assumptions.

Effort over the past year was devoted to revamping the instrumentation used in this facility. The entire laser-based data acquisition and analysis systems were re-done, with a new system purchased under a DURIP Grant. Operating procedures for the facility were revamped with benchmarking against best practices elsewhere to establish procedures that would guide laser safety procedures at Georgia Tech. The velocity fields were re-examined with new analysis software, to improve quantitative accuracy and determine the answer to the main question raised by the prior findings:

The answer to the “So-What” question is addressed in the results presented and discussed below. These are from a paper being presented at the 2nd International Forum on Rotorcraft Multidisciplinary Technology in Korea this October (Ref. 16). The blade surface in each image was located again with reference to video images taken of the blade with ordinary lighting in addition to laser sheet. Analyzing the blade dynamics suggests that the observed flapping angle implies a much smaller aerodynamic contribution than is predicted from high Reynolds number lift coefficient tables; This is reasonable given the Reynolds number range and blade aspect ratio used here.

1. Profiles of Outward Velocity at 3 Radial Stations.

The radial jet flow develops over the surface because of the rotation of the blade. However, at the blade surface, the no-slip condition must apply and hence there cannot be any radial velocity. This means that there must be a boundary layer under the radial jet flow. The radial acceleration is also experienced at the bottom surface of the blade where there is attached flow. The cross-flow velocity map should therefore show strong radial jet layers very near both surfaces, but there must also be a boundary layer right next to each surface. This boundary layer is very thin, and it is not expected that PIV will resolve this in the present experiments. Thus, what should be a double-peaked radial velocity profile with the blade surface between the two peaks, should appear instead with a single peak without the blade boundary layer seen. This is what occurs at the more inboard stations, as shown in Figures 18 and 19 below. These figures are slightly different from the radial velocity plots shown before, in that the “radial” velocity component is now changed to the component parallel to the blade surface (the blade is flapped up 4+ degrees), in order to be able to consider the vorticity in the boundary layer. In Figure 20, at the outboard station r/R = 0.814, the split into two profiles can be clearly seen. It must be noted that these are instantaneous velocity realizations.

Constructing the average of 100 such plots is difficult because there is a substantial difference between those instants when two peaks can be seen, and those where only one can be seen. In general, at outboard stations like r/R=0.814, the double peak is seen more frequently than the single peak, whereas at more inboard locations the opposite is true.

From these plots, a reasonable estimate may be made of the peak "radial" (here meaning parallel to the blade surface) velocity reached in the jet near the surface. The upper part of the jet shear layer in the recirculating flow region can also be seen from the figures. The vorticity of this part of the profile can be quantified. However, this does not give a fair indication of the amount of vorticity in the surface boundary layer.

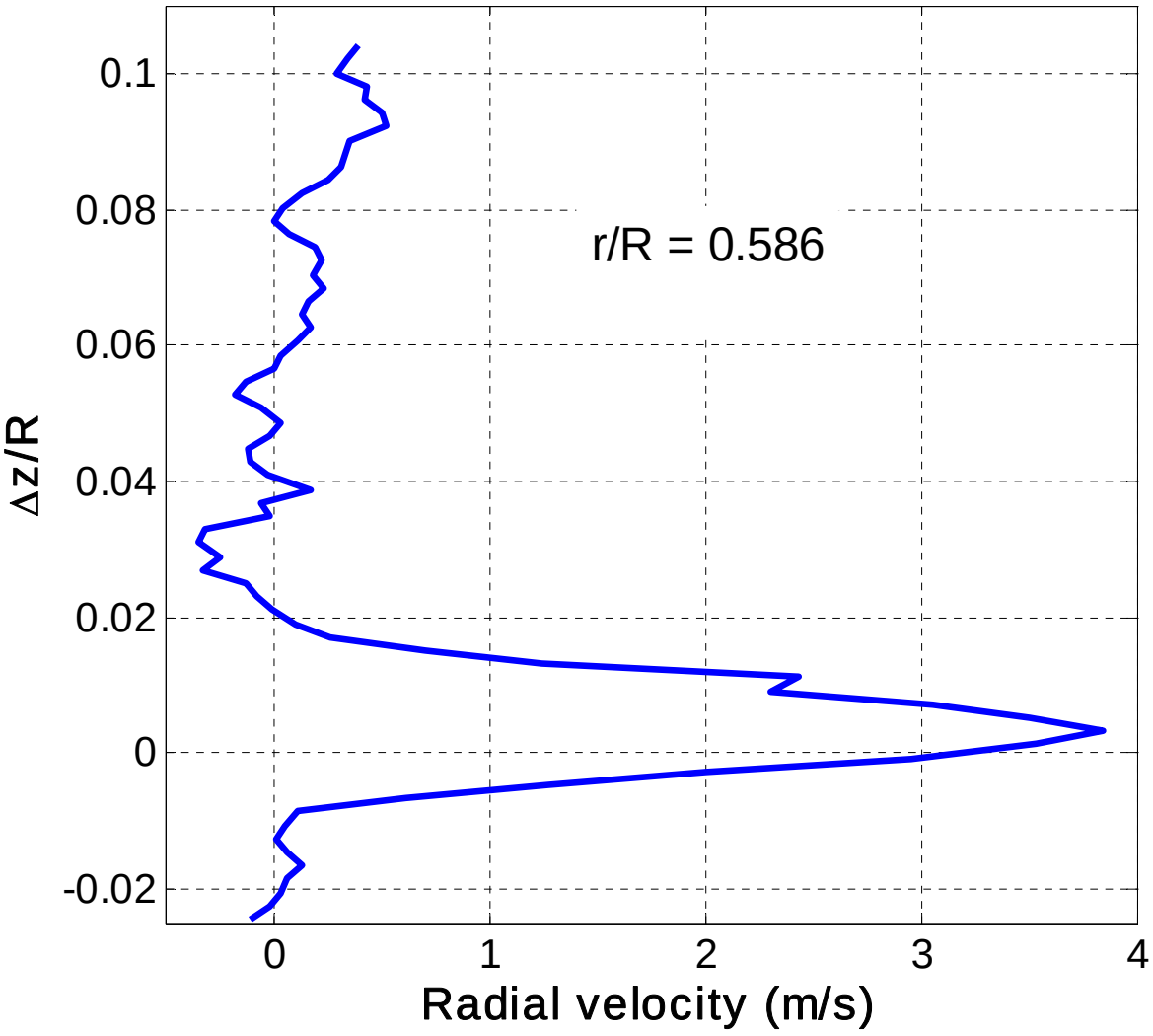

Figure 18: Velocity profile of the component of velocity along the surface of the blade, at r/R=0.586.

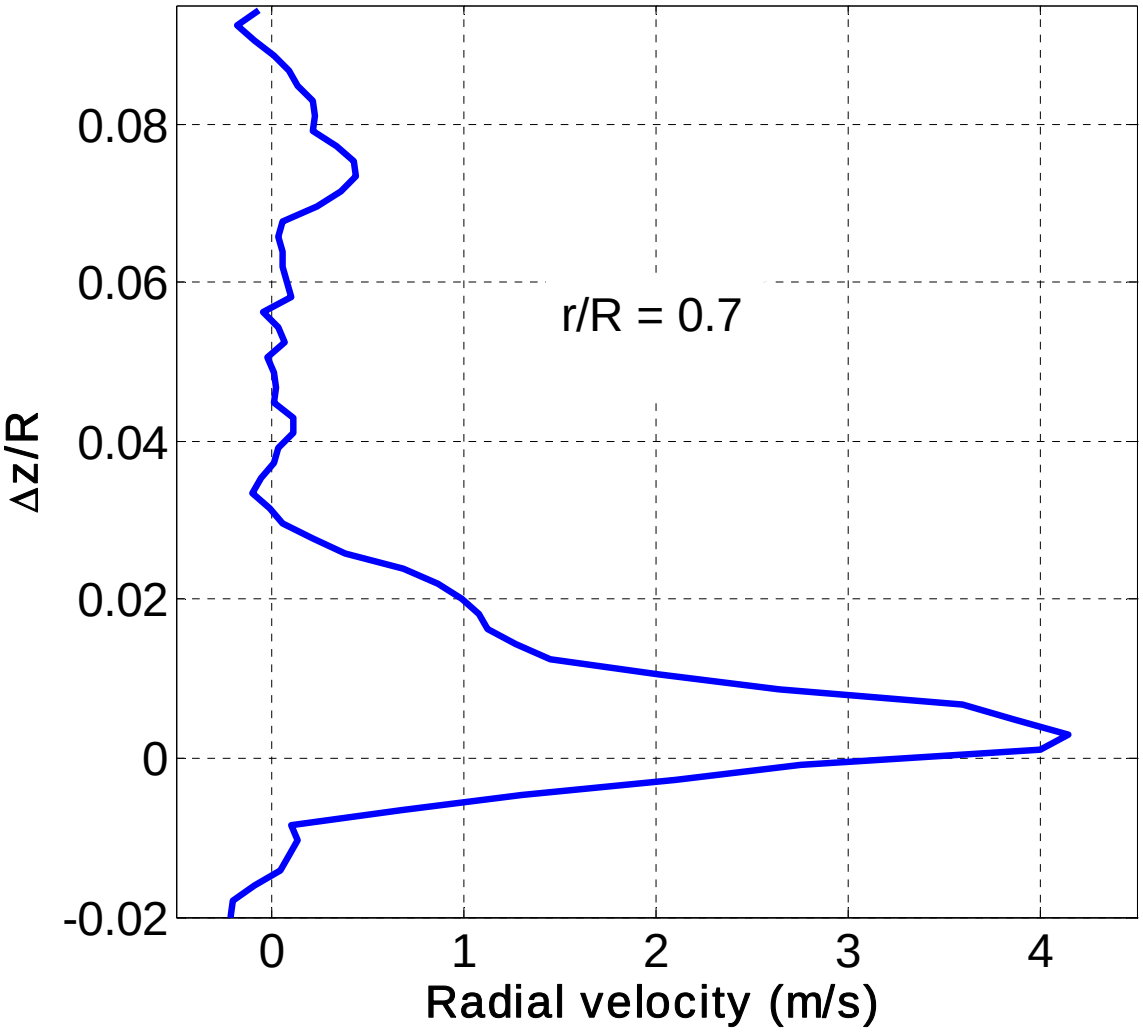

Figure 19: Velocity profile of the component of velocity along the surface of the blade, at r/R=0.7

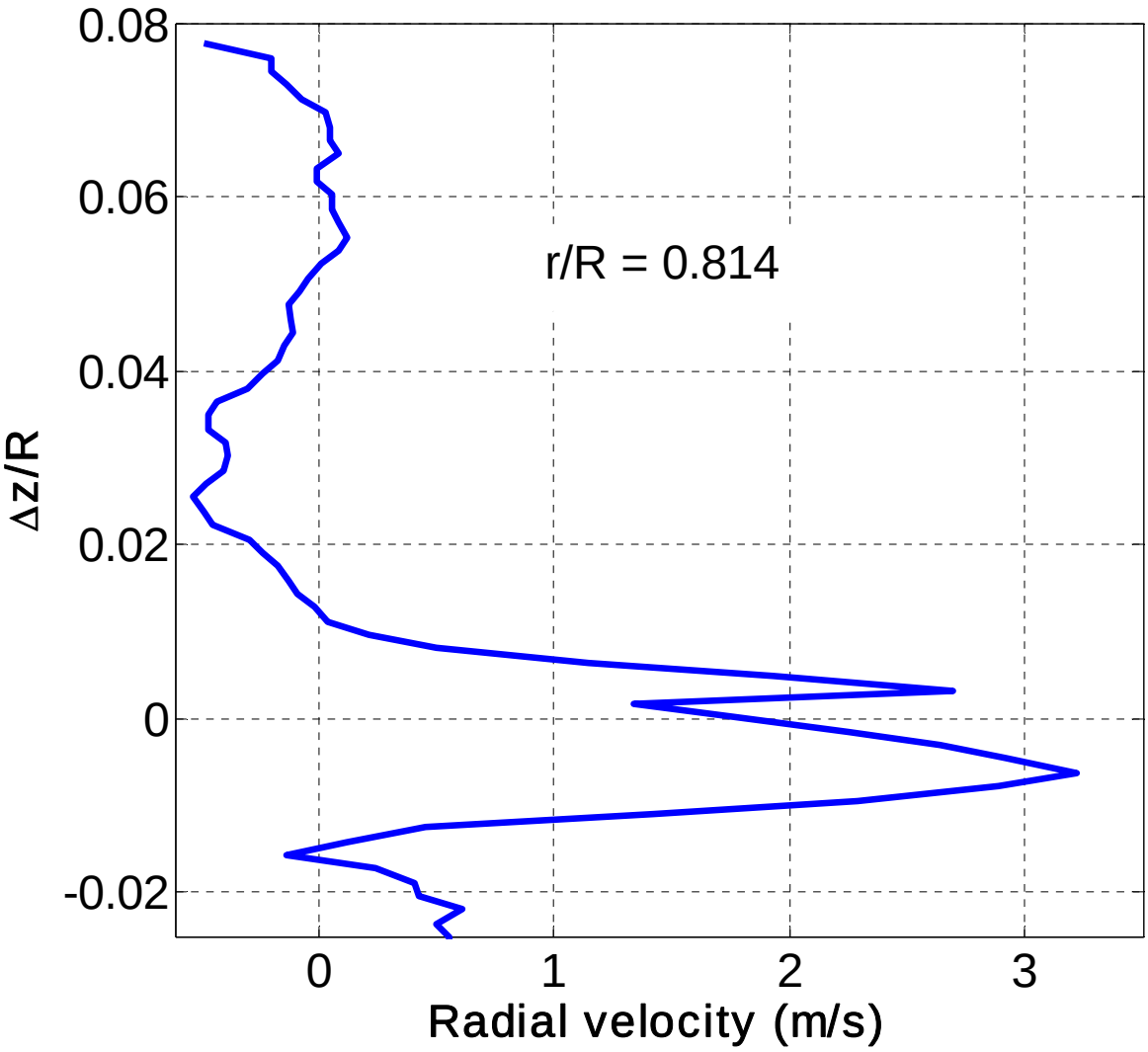

Figure 20: Velocity profile of the component of velocity along the surface of the blade, at r/R=0.814

Vorticity Contours Quantified in the Crossflow Plane Over the Blade.

Now we revisit the vorticity contours of the discrete structures. Figure 21 shows the vorticity contours in the cross-flow plane. It is clear that the overall jet shear layer has broken into 5 discrete structures in the radial window from 0.5R to 0.67R. In the window centered at r/R = 0.7 (Figure 21), the breakup is clearer and the peak vorticity exceeds 300 /s. In Figure 22, centered around r/R=0.814, the peak vorticity in the discrete structures exceeds 500 /s. The shear layer seems to be lifting off the surface entirely.

Quantitative analysis of the vorticity shows that the discrete structures account for 30% or more of the vorticity in the shear layer from the peak of the radial jet layer, to the rest of the recirculating zone. Thus the breakup certainly prevents further strengthening of the jet layer, and must have a profound influence on the flow direction and magnitude near the bottom of the recirculating flow. In turn, this must have a significant effect on pressure coefficient and on lift and pitching moment coefficients.

A true estimate of how much of the surface-generated vorticity is removed from the jet layer by the discrete structures, must await better resolution and calculation of the surface boundary layer. Some estimate of this boundary layer thickness may be derived from plots such as that in Figure 19 at the outer stations, but these will overestimate the thickness and thus underestimate the vorticity at the inboard stations.

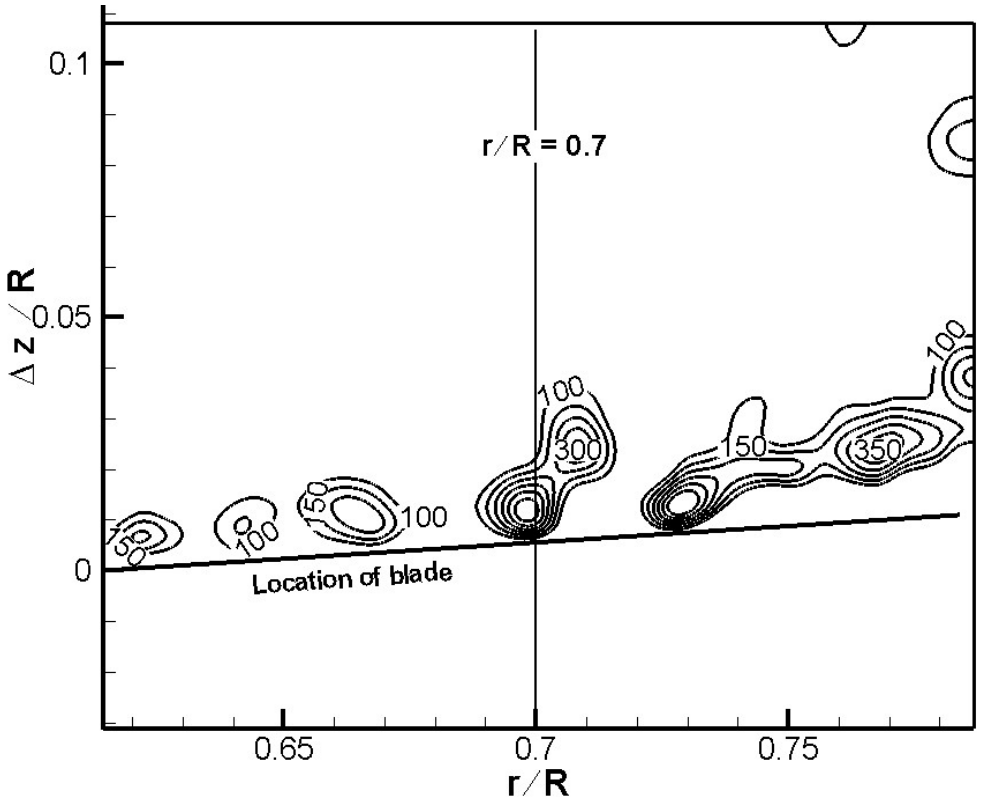

Figure 21: Contours of vorticity in the cross-flow plane, centered at r/R=0.7.

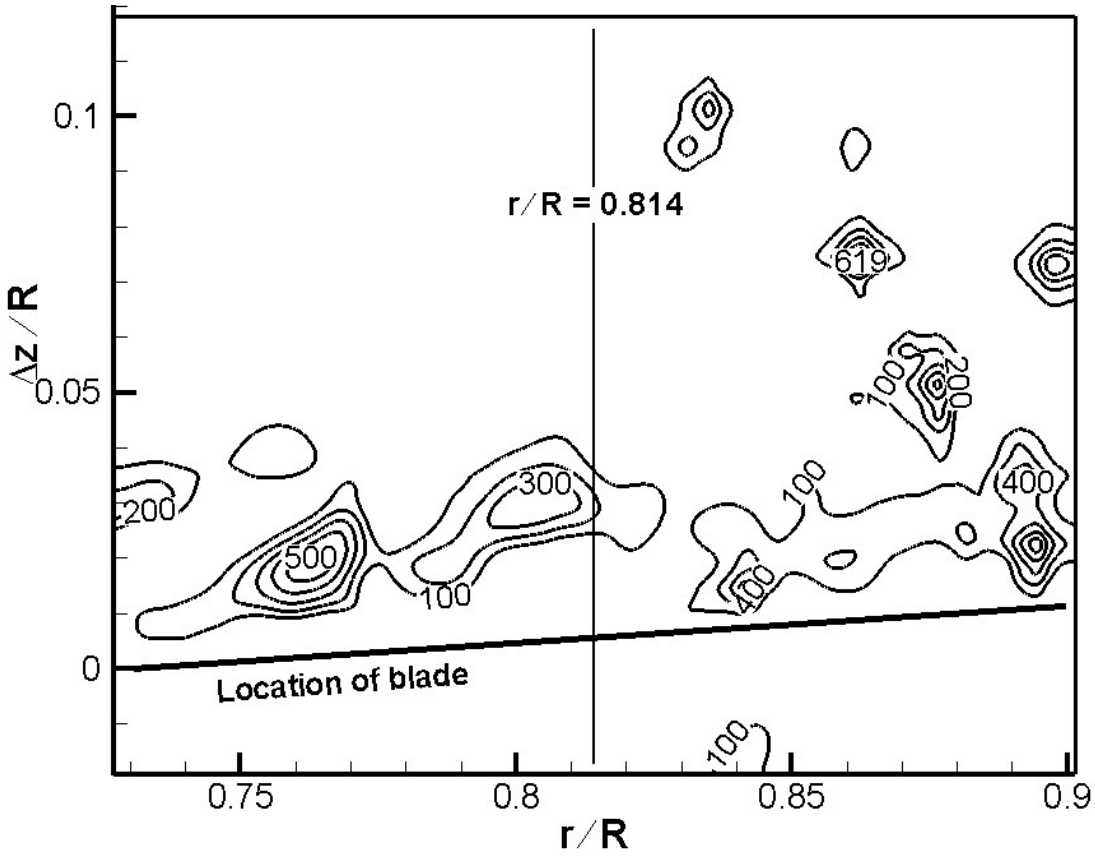

Figure 22: Contours of vorticity in the cross-flow plane centered at r/R=0.814

Chordwise Progression

Results from other cross flow planes further along the chord towards the separation line are shown in the following figures. In Figures 23 and 24 showing velocity profiles at the r/R=0.586 station at different chordwise locations, the blade surface location cannot be precisely identified from the test data. Scattering of laser light from the surface heavily contaminated the scattering from seed particles in this region. Thus the peak radial velocity is assumed to be essentially at the blade, and no conclusions can be derived regarding the blade surface boundary layer. Data below that are arbitrarily set to zero velocity. Accordingly, the zero for the z axis cannot be set precisely. Again only the single peak is seen. The peak radial velocity is higher at the more forward stations, that is, closer to the separation line, reaching well over 5 m/s at x/c = 0.428(Figure 24) compared to only 3.8 at the trailing edge and 4.4 at x/c=0.714 (Figure 23). Figures 25 and 26 present similar trends at r/R = 0.7 and 0.814 respectively.

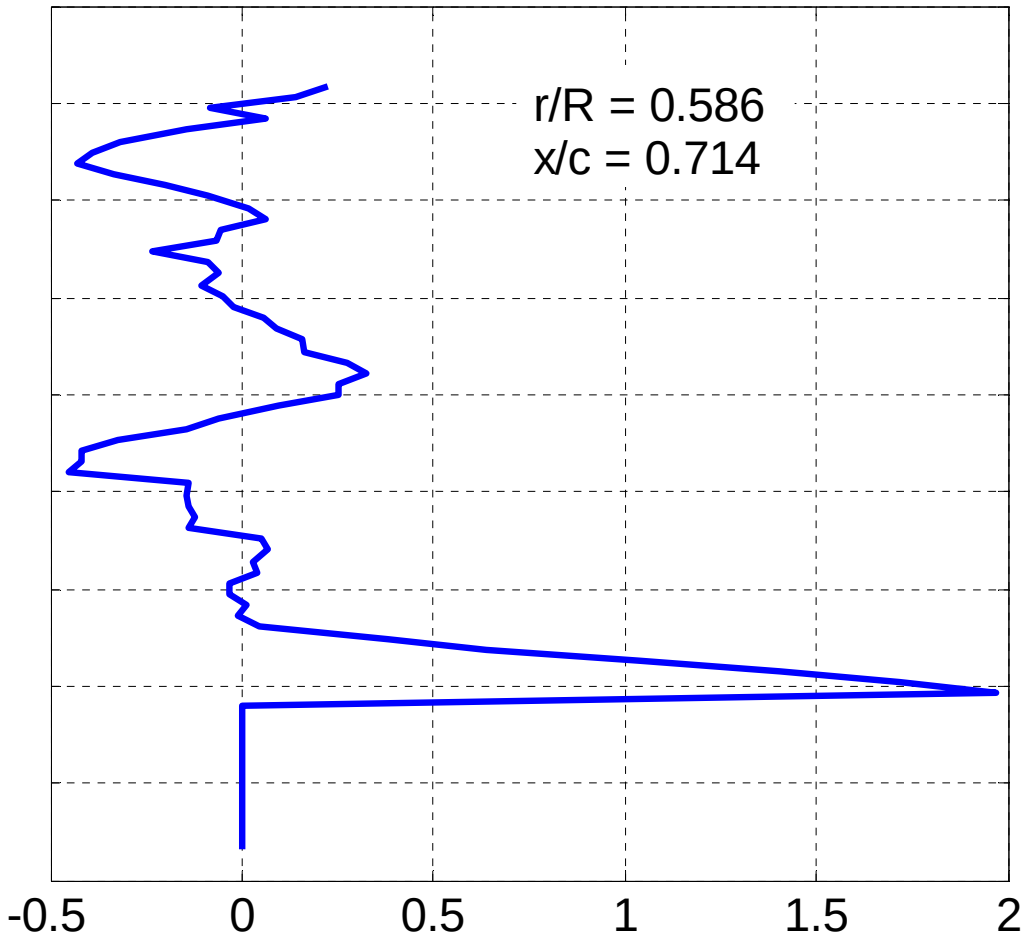

Figure 23: Profile of radial velocity in m/s at x/c=0.714, r/R=0.586. There are no data below the location of peak radial velocity.

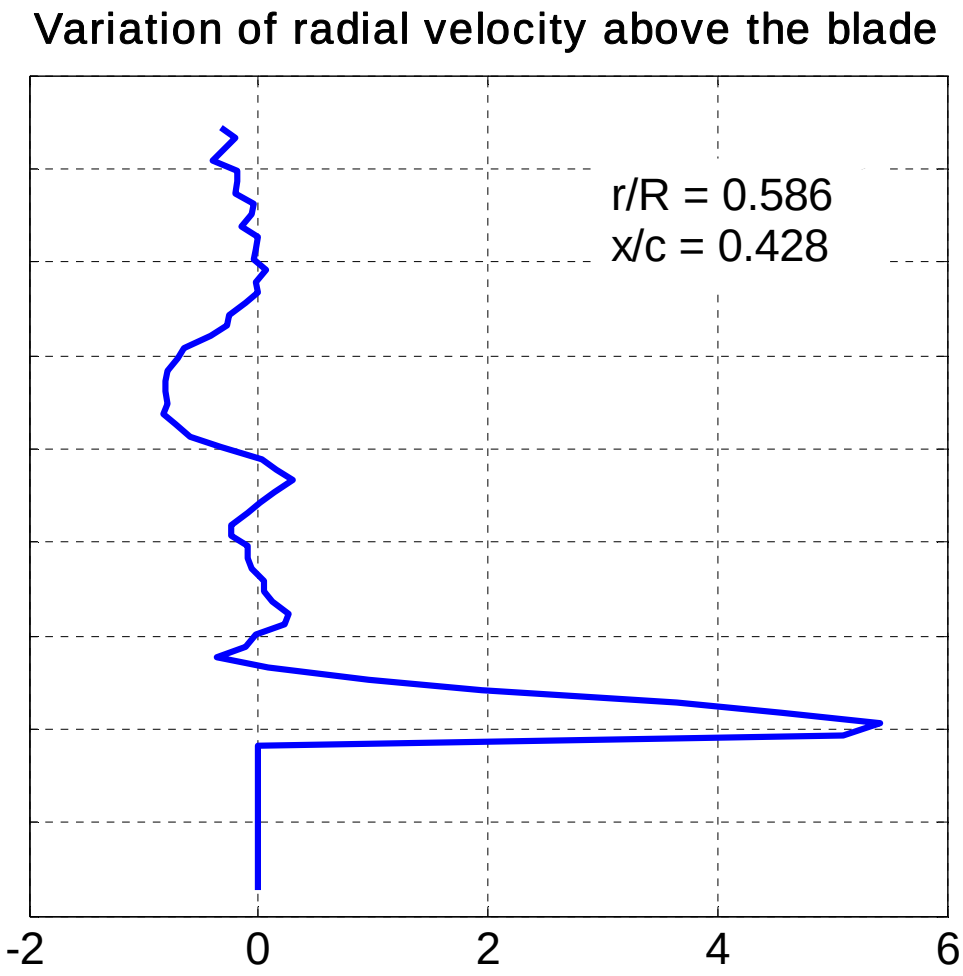

Figure 24: Profile of radial velocity in m/s at x/c=0.428, r/R=0.586. There are no data below the location of peak radial velocity.

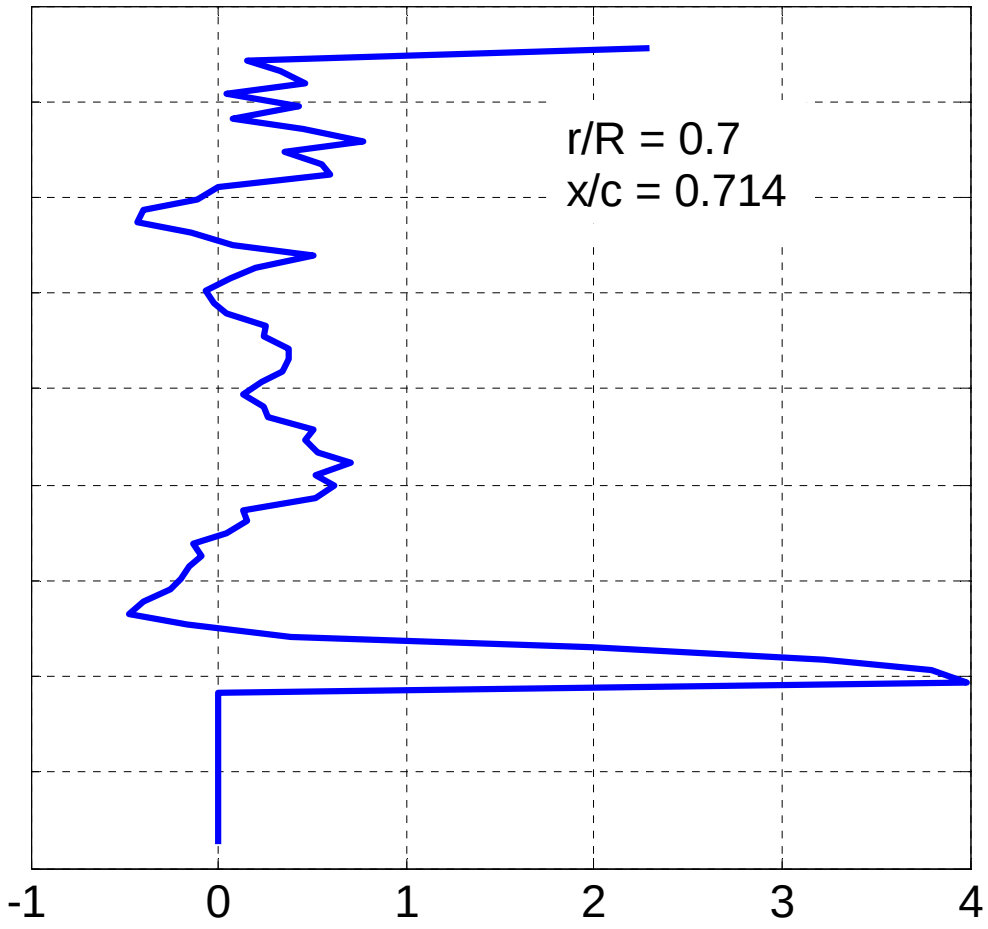

Figure 25: Profile of radial velocity in m/s at r/R=0.7, x/c=0.714

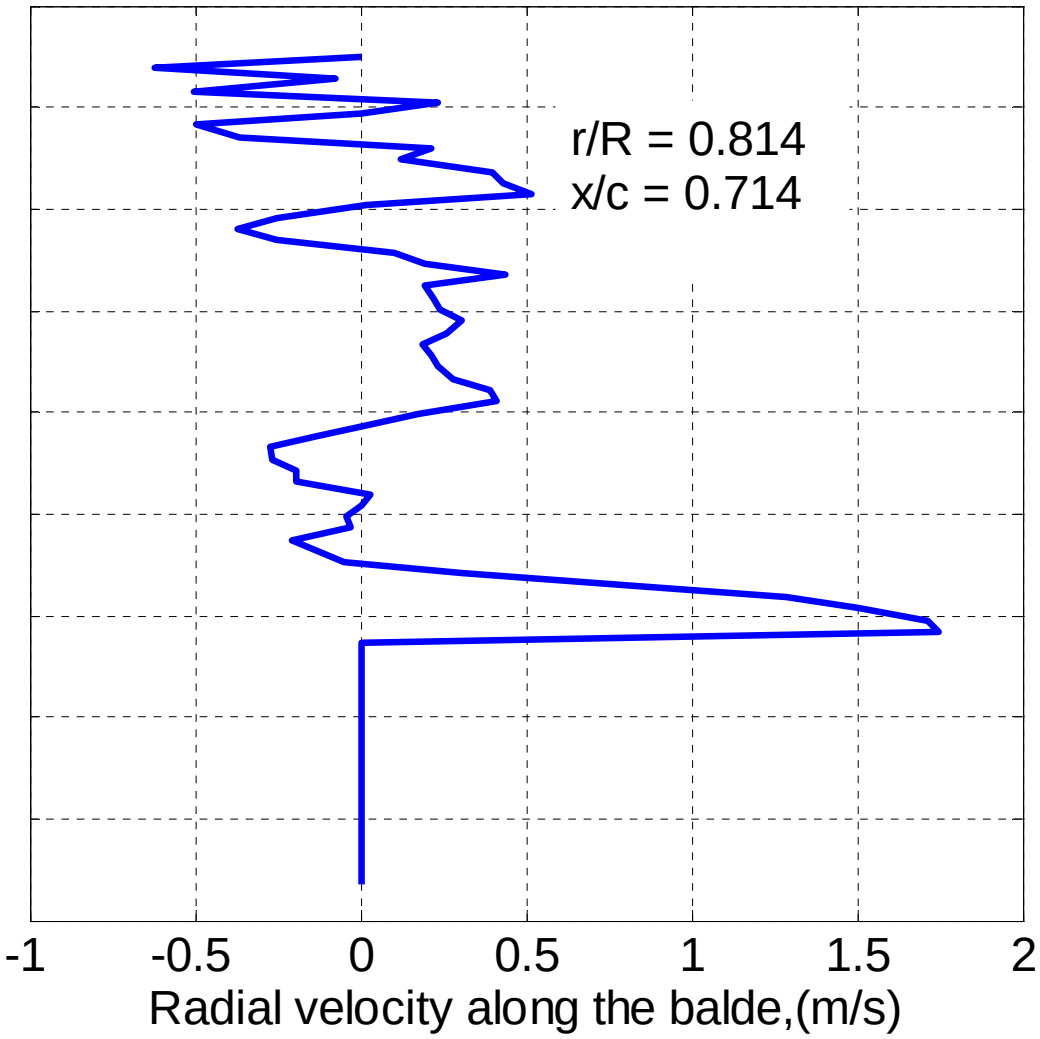

Figure 26: Profile of radial velocity at r/R=0.814, x/c=0.714

Vorticity contours in the crossflow plane as before, show discrete structures. Figure 27 shows vorticity in the window centered at r/R=0.586 at x/c=0.714. The structures are not significantly different from those seen at the trailing edge plane. However, at x/c=0.428, shown in Figure 28, the magnitude of vorticity appears to be substantially higher. This corresponds to the higher peak radial velocity seen in the near-surface jet at this station. Similar trends are seen at the r/R = 0.7 and 0.814 locations, shown in Figures 29 and 30 respectively.

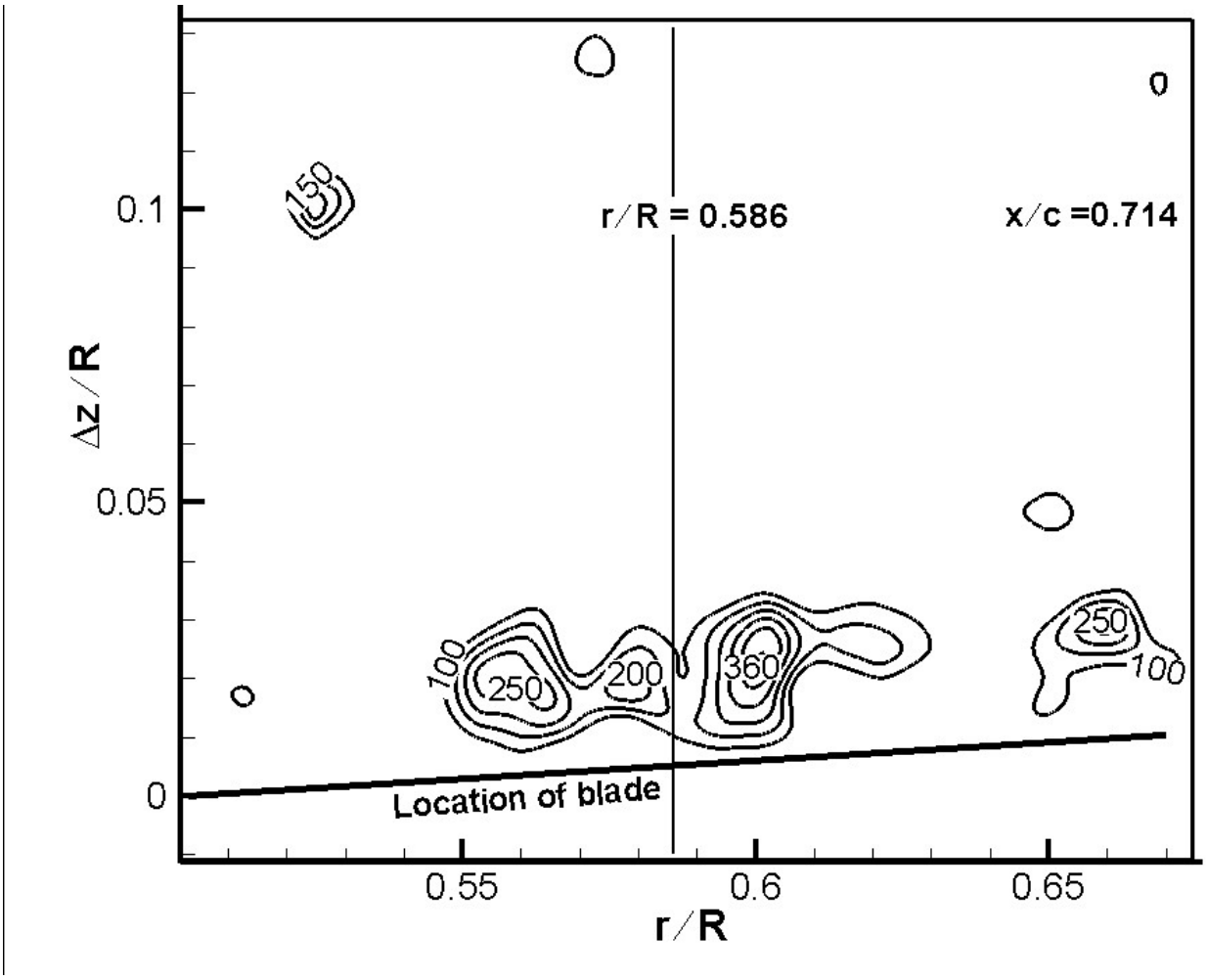

Figure 27: Vorticity Contours in the crossflow plane at x/c=0.714, centered at r/R=0.586

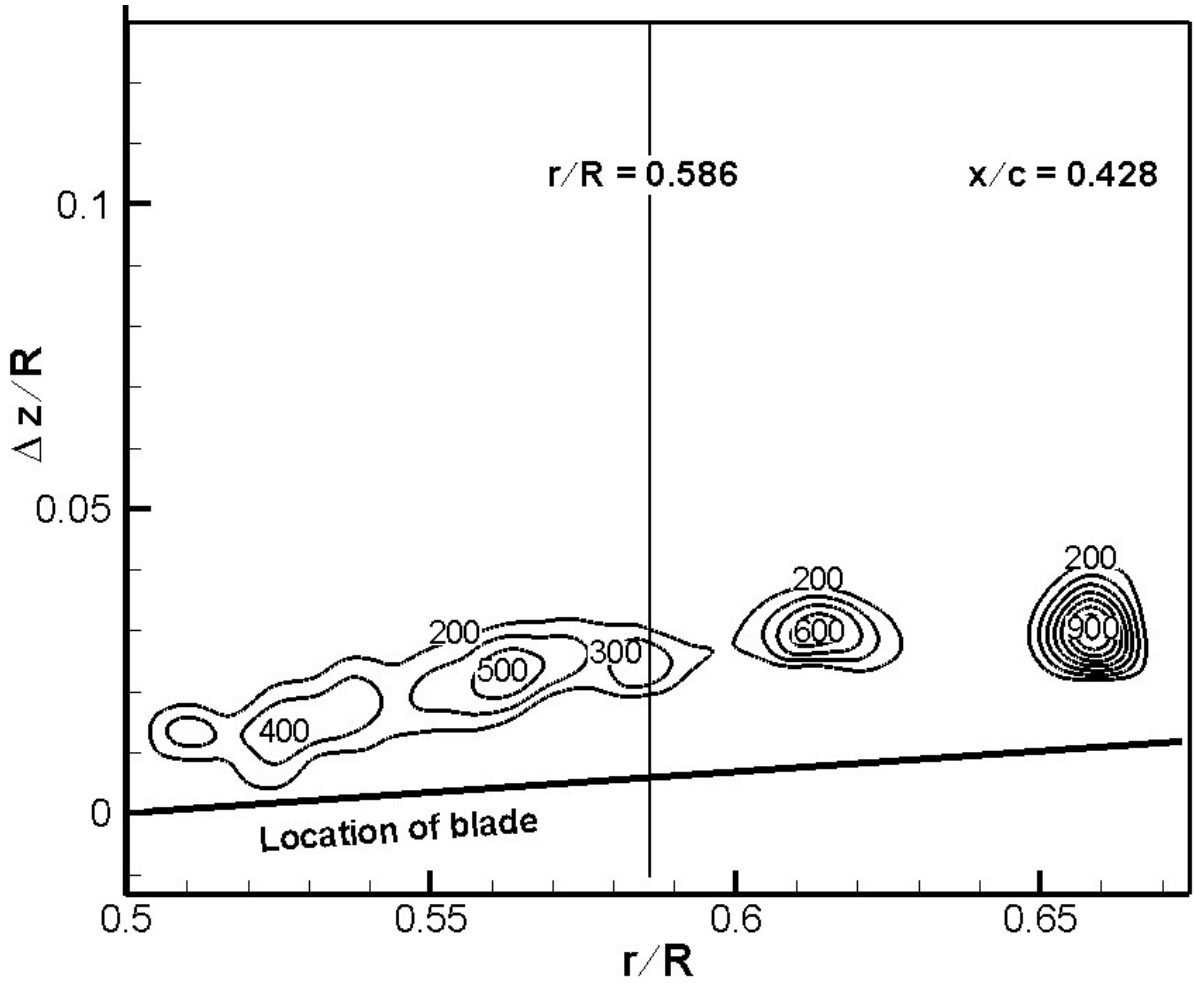

Figure 28: Vorticity Contours in the crossflow plane at x/c=0.428, centered at r/R=0.586

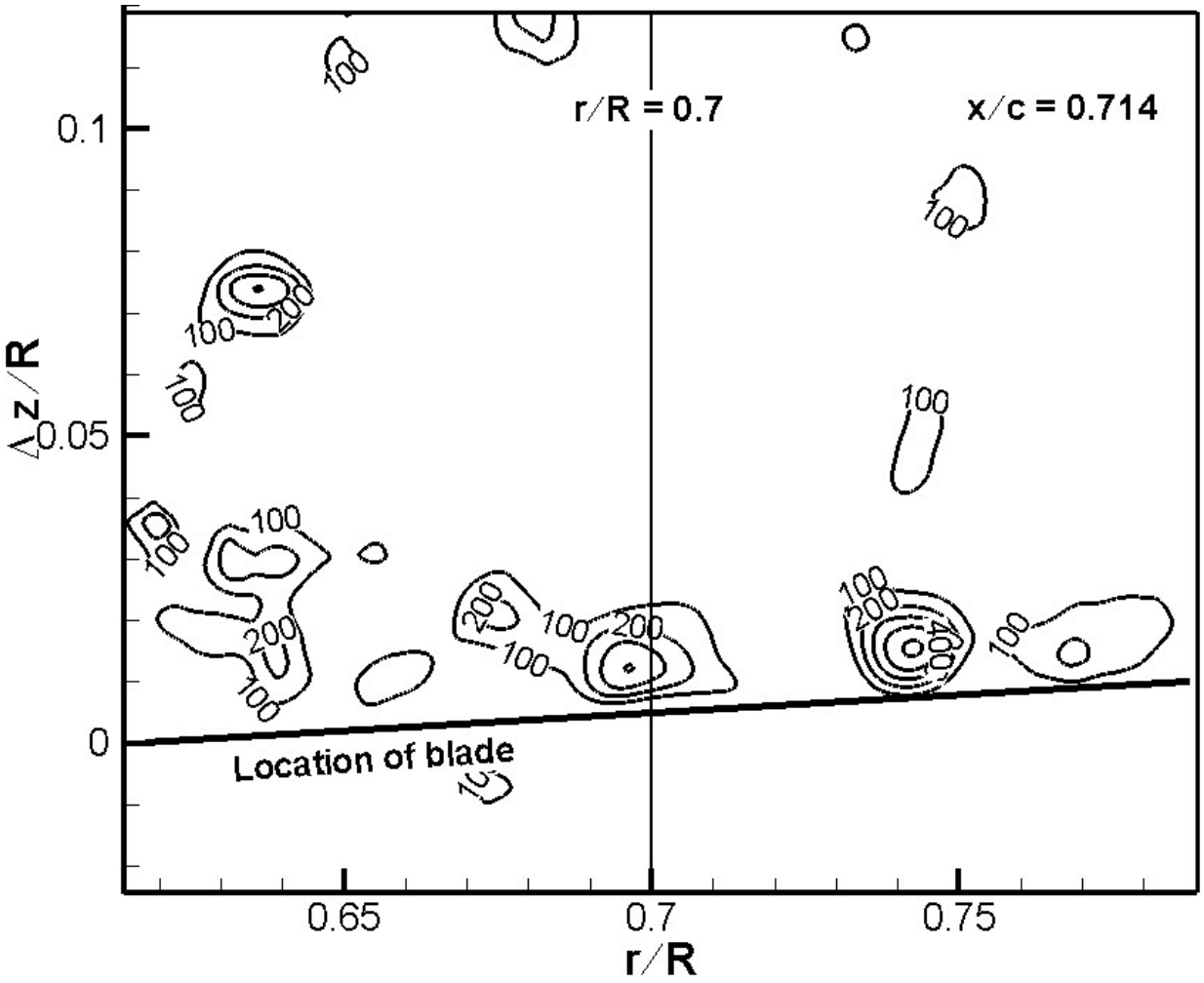

Figure 29: Vorticity contours in the crossflow plane at x/c=0.714, centered at r/R=0.7

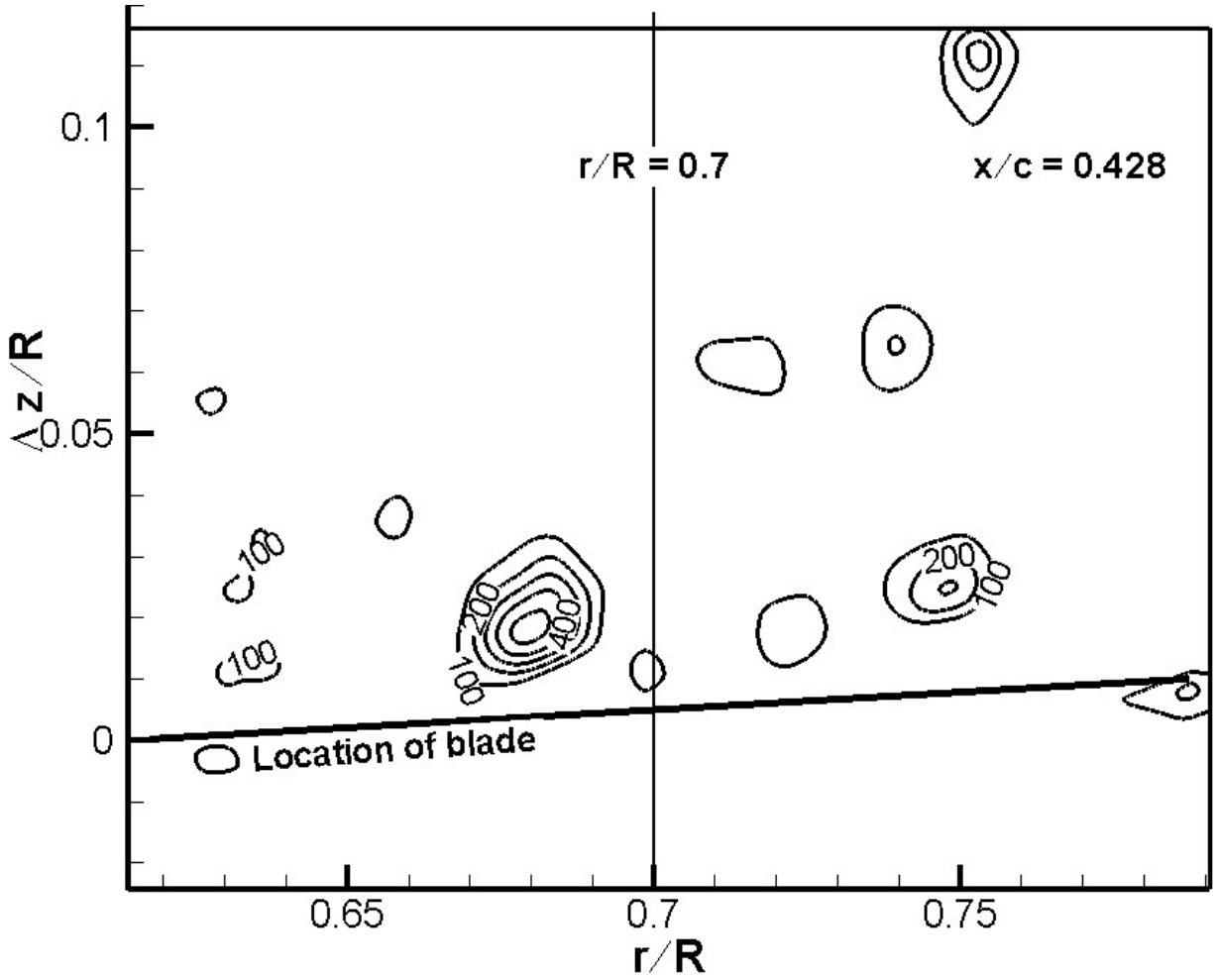

Figure 30: Vorticity Contours in the crossflow plane at x/c=0.428, centered at r/R=7

Figures 31 and 32 summarize these trends. The average value of the radial velocity peak over 100 images is seen to decrease as one moves outboard at a given chordwise station. This is contrary to what one might expect if no vorticity were leaving the radial jet. It cannot be explained by reasoning that the radial jet one sees at a given radial station, in fact originated at a different radial location at a more forward chordwise station. Figure 32 indicates that there is no systematic variation in the peak of the averaged radial velocity profile, with chordwise distance. Hence the result in Figure 31 must at this stage be interpreted to mean that the radial jet strength is very substantially depleted by the formation and breaking away of the discrete vortical structures. Now we are much more strengthened in ascribing the difference between expected radial flow, and the observed weak effects of radial flow in load predictions. In other words, any "success" of prediction techniques that ignore the radial flow must be viewed as being entirely fortuitous, and not based on a realistic depiction of the fluid dynamics.

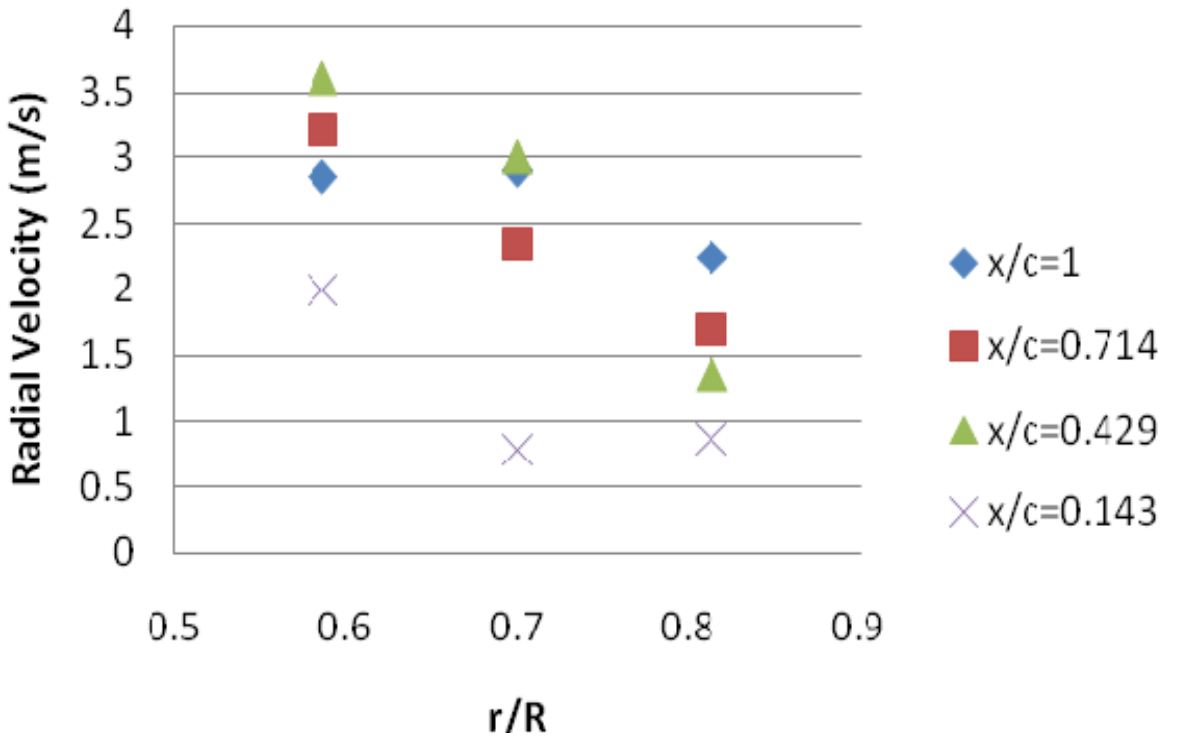

Figure 10: : Radial Velocity vs. Spanwise Location

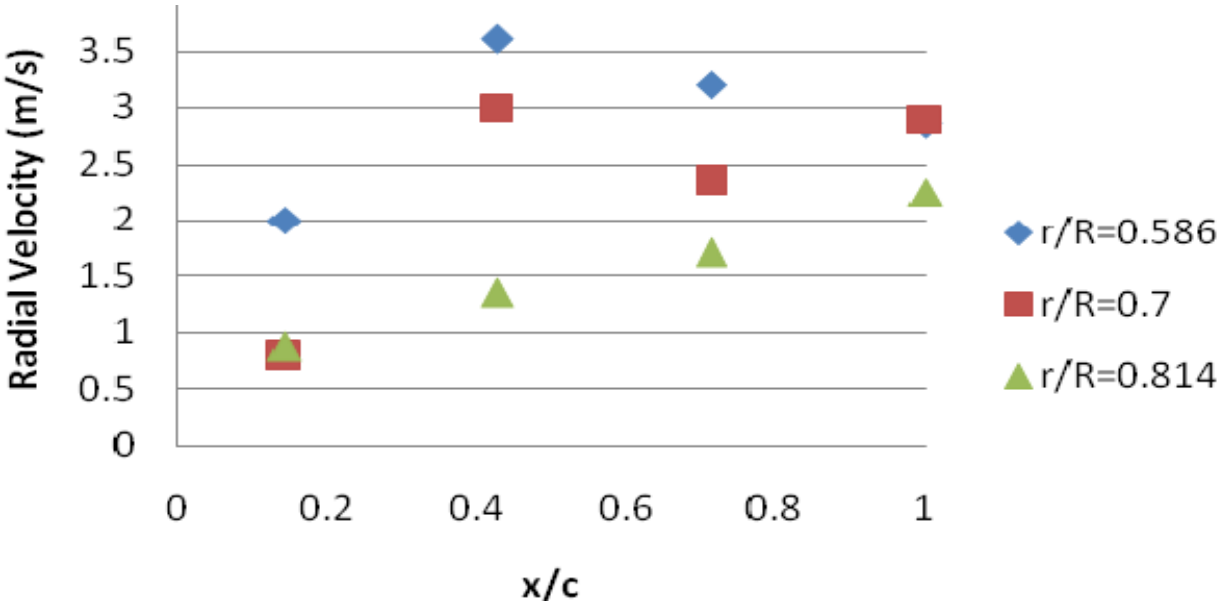

Figure 11: Radial Velocity vs. Chordwise Location

6. CONCLUSIONS

1. A single-blade hover facility has been used to study temporal evolution of flow close to a rotating blade. An Inflow Obstructor is validated as a method of inducing transient stall to simulate dynamic stall features downstream of the separation line.
2. PLIS and PIV verify occurrence of stall based on stoppage of through-flow.
3. Downstream of the stall line in the inflow obstructor case, radial velocity along the blade sharply develops an outward direction. However, the formation of stall cells along the radius exchanges fluid away from the blade boundary layer.
4. Time-varying cells of radial flow separation in the inflow obstructor case, comparable in scale to blade chord, occur in the flowfield downstream of the stall line. These are not phase-locked to the rotor azimuth.
5. The same form of structures appears clearly in the forward flight dynamic stall flowfield. Co-rotating structures similar to a shear layer appear, and suggest that the free shear layer formed at stall, rolls up into discrete structures, or cells. However, actual upflow regions are not observed.
6. The spanwise spacing of structures is approximately the height of the separated flow region.
7. Radial velocity profiles show strong radial flow inboard, and weaker radial flow at outboard stations, corresponding to the expectation of deep stall inboard and attached flow near the tip.
8. The boundary layer under the radial flow is captured in the PIV data.
9. The radial flow profile appears to be fairly repeatable near the surface. However, above this region, the velocity profile is not repeatable from one cycle to another.
10. The discrete vortical structures carry on the order of 30% of the vorticity in the shear layer between the radial jet and the recirculating zone.
11. At outboard stations, the jet and the discrete strucures lift off the surface, allowing capture of the boundary layer between the jet peak and the blade surface.
12. This, as far as we know, is the first capture and measurement of the quasi-periodic radial velocity field on a rotating blade, and in particular of the profile of the strong radial velocity above a rotating blade in stall.
13. The occurrence of discrete quasi-periodic but spatially repeatable vortical structures in this type of flow is also captured for the first time.
14. The magnitude comparisons show that the radial jet development, the limiting of its strength by the breakup into discrete structures, and the discrete structures themselves, are first-order phenomena in the flowfield of the rotor blade in retreating blade stall, and must have profound effects on the lift and pitching moment of the blade through stall region.
15. Averaged radial velocity profile data show that the averaged peak radial velocity decreases with increasing radial distance at a given chordwise location, contrary to what would be expected in the absence of the formation and breakup of discrete vortical structures. Thus any agreement of computational predictions that ignore the radial acceleration and resulting flow, with measured airloads in dynamic stall, must be viewed as fortuitous, and not representative of the true fluid dynamics of the problem.

8. REFERENCES

1. Lorber, P., McCormick, D., Anderson, T., Wake, B., McMartin, D., Pollack, M., Corke, T., and Breuer, K., “Rotorcraft Retreating Blade Stall Control," AIAA Paper 2000-2475.
2. Carr, L. W., “Progress in Analysis and Prediction of Dynamic Stall," Journal of Aircraft, Vol. 25, No. 1, January 1988, pp. 6-17.
3. Bousman, W., “A Quantitative Examination of Dynamic Stall from Flight Test Data," Proceedings of the AHS Forum, May 1997, pp. 368-387.
4. Coton, F. N., Wang, T., and Galbraith, R. A., “An Examination of Key Aerodynamic Modelling Issues Raised by the NREL Blind Comparison," Wind Energy, Vol. 5, 2002, pp. 199-212.
5. Corten, G., “Flow Separation on Wind Turbine Blades”, Doctoral dissertation, University of Utrecht, 2001.
6. Xu, G. and Sankar, L. N., “Effects of Transition, Turbulence, and Yaw on the Performance of Horizontal Axis Wind Turbines," AIAA Paper 2000- 0048, 38th AIAA Aerospace Sciences Meeting and Exhibit, Reno, NV., January 2000.
7. Komerath, N., Liou, S.-G., and Hyun, J.-S., “Flowfield of a Swept Blade Tip at High Pitch Angles," Paper 91-0704, AIAA, January 1991.
8. Yang, J., Ganesh, B., and Komerath, N., “Radial Flow Measurements Downstream of Forced Dynamic Separation on a Rotor Blade," Paper 2006-3377, AIAA, June 2006.
9. Gregory, N., Quincy, V. G., O'Reilly, C. L., and Hall, D. J., “Progress Report on Observations of Three Dimensional Flow Patterns Obtained During Stall Development on Aerofoils, and on the Problem of Measuring Two-Dimensional Characteristics". NPLAero Report 1309, Aeronautical Research Council, Fluid Motion Sub-Committee, 1970.
10. Winkelmann, A. E. and Barlow, J. B., \Flow eld Model for a Rectangular Planform Wing Beyond Stall," AIAA Journal, Vol. 18, No. 8, 1980, pp. 1006{1008.
11. Weihs, D. and Katz, J., “Cellular Patterns in Poststall Flow over Unswept Wings," AIAA Journal, Vol. 21, No. 12, 1983, pp. 1757{1758.
12. Yon, S., “Coherent Structures in the Wake of a Stalled Rectangular Wing”, Ph.D. thesis, University of California, San Diego, and San Diego State University, 1995.
13. Yon, S. and Katz, J., “Cellular Structures in the Flow Over the Flap of a Two-Element Wing," CR 97-112613, NASA, 1997.
14. Broeren, A. and Bragg, M., “Spanwise Variation in the Unsteady Stalling Flowfield of Two-Dimensional Airfoils," Paper 2001-0861, AIAA, 2001.
15. DiOttavio, J., Watson, K., Komerath, N., and Kondor, S., “Discrete Structures in the Radial Flow Over a Rotor Blade in Dynamic Stall," Paper 2008-7344, AIAA, 2008.